Towards Constraint-aware Learning for Resource Allocation in NFV Networks

Tianfu Wang [1] **Long Yang** [2] **Chao Wang** [1] **Chuan Qin** [3] **Liwei Deng** [4] **Li Shen** [5] **Hui Xiong** [3]

Abstract

Virtual Network Embedding (VNE) is a fundamental resource allocation challenge that is associated with hard and multifaceted constraints in network function virtualization (NFV). Existing works for VNE struggle to handle such complex constraints, leading to compromised system performance and stability. In this paper, we propose a **CON**straint-**A**ware **L**earning framework, named **CONAL**, for efficient constraint handling in VNE. Concretely, we formulate the VNE problem as a constrained Markov decision process with violation tolerance, enabling precise assessments of both solution quality and constraint violations. To achieve the persistent zero violation to guarantee solutions' feasibility, we propose a reachability-guided optimization with an adaptive reachability budget method. This method also stabilizes policy optimization by appropriately handling scenarios with no feasible solutions. Furthermore, we propose a constraint-aware graph representation method to efficiently learn cross-graph relations and constrained path connectivity in VNE. Finally, extensive experimental results demonstrate the superiority of our proposed method over state-of-the-art baselines. Our code is available at https://github.com/GeminiLight/conal-vne.

1. Introduction

Network Function Virtualization (NFV) is a promising technique that facilitates the deployment of multiple Virtual Networks (VNs) tailored to user network demands within a shared Physical Network (PN) infrastructure (Yi et al., 2018). It is vital for domains such as cloud computing, edge computing and 5G, where dynamic and efficient resource management is essential (Zhuang et al., 2020). Virtual Network Embedding (VNE), a fundamental resource allocation problem in NFV, is critical for maintaining high Quality of Service (QoS). This process, involving the mapping of VNs to PNs, represents a significant challenge. It is an NP-hard Combinatorial Optimization Problem (COP) characterized by intricate and hard constraints (Rost & Schmid, 2020).

Traditional solutions to VNE ranging from exact to heuristic methods often suffer from either expensive computation times or limited performance in complex network scenarios (Zhang et al., 2018; Fan et al., 2023). Recently, Reinforcement Learning (RL) has been a potential direction for VNE, which learns effective solving policies without relying on high-quality labeled data. Typically, existing RL-based methods solve the VNE problem as a Markov Decision Process (MDP) (Haeri & Trajković, 2017; Yan et al., 2020; Zhang et al., 2024b), where a neural policy is iteratively optimized through interactions with an environment. They construct VNE solutions by sequentially selecting an available physical node to place each virtual node, until the solution is completed or constraints are violated. However, the hard constraints of VNE require a persistent zero-violation at each decision timestep, which results in numerous *failure samples* where constraints are violated during training. For *failure samples*, existing studies (e.g., Yao et al. (2020); Zhang et al. (2022)) consider them as noisy and only train with data that violate no constraint; or others, like Yan et al. (2020) and He et al. (2023a), consider fixed penalties to them and discourage violations.

Although these RL-based algorithms (Zhang et al., 2022; He et al., 2023a; Zhang et al., 2024b) have shown efficacy, they still suffer from several significant problems in handling complex constraints of VNE. Firstly, ignoring *failure samples* makes policies prone to violating critical constraints, while employing fixed penalties in reward signals does not accurately reflect the severity of constraint violations. Thus, these methods underestimate valuable sample information and hamper the learning of constraint-aware policies, which results in low feasibility guarantees. Secondly, it is hard to avoid to encounter *unsolvable instances* whose feasible sets are empty in practical scenarios, due to insufficient physical resource availability or excessive virtual resource requests. It is impractical to distinguish solvable and *unsolvable instances*, since checking the instance solvability of an NP-hard problem is time-consuming. *Failure samples* caused by *unsolvable instances* further complicate the constraint learning process, and negatively impact the stability of training and policy performance. See Appendix C for a preliminary study, which highlights the negative impact

[1]USTC [2]PKU [3]HKUST (GZ) [4]UESTC [5]SYSU. Correspondence to: Hui Xiong <xionghui@ust.hk>.

of unsolvable instances on training stability. Thirdly, VNE constraints are complex and multifaceted, involving cross-graph status interactions and bandwidth-constrained path connectivity assessments, which are not adequately captured by the feature extractors used in current studies.

To address these challenges, we propose a **CON**straint-**A**ware **L**earning framework for VNE, named **CONAL**, achieving high solution feasibility guarantee and training stability. Concretely, to optimize performance while enhancing constraint satisfaction, we formulate the VNE problem as Constrained MDP (CMDP) (Altman, 2021) with violation-tolerance. Although constraint violations often trigger early termination during solution construction, leading to incomplete solutions and complicating the measurement of both solution quality and violation degree, this method enables complete solution construction and precise measurement. Additionally, we introduce a reachability analysis into the optimization objective to achieve persistent zero constraint violation required by VNE. To handle the existence of *unsolvable instances* whose constraints are impossibly satisfied, we propose an adaptive reachability budget method to make the policy optimization more stable. It dynamically decides the violations caused by a surrogate policy as budgets based on the instance's solvability, rather than always setting budgets to zero. Furthermore, to finely perceive the complex constraints of VNE, we propose a constraint-aware graph representation method tailored for VNE, which includes a heterogeneous modeling module for cross-graph status interactions. We also devise several feasibility-consistency augmentations and utilize contrastive learning to bring representations under different views close, which enhances the sensitivity of policy towards path-bandwidth constraints.

Our main contributions are summarized as follows: (1) We propose a violation-tolerant CMDP modeling approach for VNE, which precisely evaluates the quality of solution and the degree of constraint violation. To achieve persistent zero constraint violation, we also present a reachability-guided optimization objective. (2) We present a pioneering work on the study of unsolvable instances negatively impacting the stability of policy optimization in COP, and propose a novel adaptive reachability budget method to handle such challenges. (3) We propose a constraint-aware graph representation method tailored for VNE, where a path-bandwidth contrast module with feasibility-consistency augmentations perceives connectivity at a fine-grained level. (4) We conduct extensive experiments in various network scenarios, showing the CONAL's superiority on performance, training stability, generalization, scalability and practicability.

2. Problem Definition

System Modeling. In real-world network systems, as illustrated in Figure 1, user network services are virtualized as VN requests that continuously seek resources from the PN.

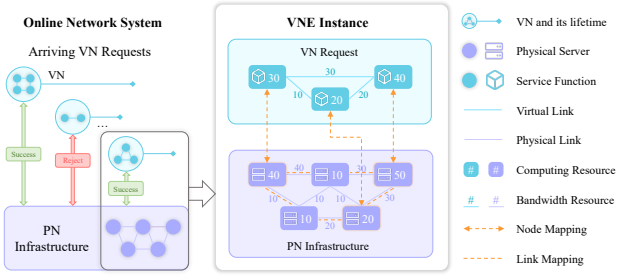

Figure 1: A brief example of VNE problem. In the network system, VN requests arrive sequentially at the infrastructure to require the resources of PN. For the VNE instance, embedding a VN to the PN consists of node and link mapping processes, while considering intricate and hard constraints.

Each arrived VN request, along with the current situation of the PN, constitutes an instance I, and we collect all such instances with a set $\mathcal{I}$. For each instance, $I = (\mathcal{G}_v, \mathcal{G}_p) \in \mathcal{I}$, where the PN $\mathcal{G}_p$ and VN $\mathcal{G}_v$ are modeled as undirected graphs, $\mathcal{G}_p = (N_p, L_p)$ and $\mathcal{G}_v = (N_v, L_v, \omega, \varpi)$, respectively. Here, N_p and L_p denote the sets of physical nodes and links, indicating servers and their interconnections; N_v and L_v denote the sets of virtual nodes and links, representing services and their relationships; ω and ϖ denote the arrival time and lifetime of VN request. We denote $\mathcal{C}(n_p)$ as the computing resource availability for the physical node $n_p \in N_p$, and $\mathcal{B}(l_p)$ as the bandwidth resource availability of the physical link $l_p \in L_p$. Besides, $\mathcal{C}(n_v)$ and $\mathcal{B}(l_v)$ denote the demands for computing resource by a virtual node $n_v \in N_v$ and bandwidth resource by a virtual link $l_v \in L_v$.

Mapping Process. For each instance I, embedding a VN onto the PN can be defined as a graph mapping process, denoted $f_{\mathcal{G}} : \mathcal{G}_v \rightarrow \mathcal{G}_p{}'$, where $\mathcal{G}_p{}'$ is a subgraph of $\mathcal{G}_p$ that accommodates the VN $\mathcal{G}_v$. This process comprises two sub-processes: node mapping and link mapping, where intricate hard constraints should be satisfied. Node mapping, $f_N : n_v \rightarrow n_p$, places each virtual node n_v onto a physical node n_p, while following the one-to-one placement constraints (i.e., virtual nodes in the same VN must be placed in different physical nodes and each physical node only hosts one virtual node at most) and the computing resource availability constraints must be satisfied: $\forall n_v \in N_v, \mathcal{C}(n_v) \leq \mathcal{C}(n_p)$, where $n_p = f_N(n_v)$. Link mapping, $f_L : l_v \rightarrow p_p$, routes each virtual link through a physical path p_p that connects the physical nodes hosting the two endpoints of virtual link l_v. This process need fulfill bandwidth resource availability constraints: $\forall l_v \in L_v, \forall l_p \in p_p, \mathcal{B}(l_v) \leq \mathcal{B}(l_p)$, where $p_p = f_L(l_v)$. If violating any of these constraints, then the VN request is rejected. Once embedded, the VN's occupied resources are released until its lifetime expires.

VNE Objective. To address the randomness of the network systems, same as most existing works (e.g., Zhang et al. (2022); He et al. (2023a); Zhang et al. (2024b)), we

aim to learn an optimal mapping, $f_{\mathcal{G}}$, that maximizes the resource utilization of each VNE instance. This objective facilitates long-term resource utilization and request acceptance. Revenue-to-Consumption (R2C) ratio serves as a widely used metric to measure the quality of solution $E = f_{\mathcal{G}}(I)$:

$$\text{R2C}(E) = \varkappa \cdot (\text{REV}(E)/\text{CONS}(E)), \quad (1)$$

where $\varkappa$ is a binary variable indicating the solution's feasibility; $\varkappa = 1$ for a feasible solution and $\varkappa = 0$ otherwise. When the solution is feasible, $\text{REV}(E)$ represents the revenue from the VN, calculated as $\sum_{n_v \in N_v} \mathcal{C}(n_v) + \sum_{l_v \in l_v} \mathcal{B}(l_v)$. If $\varkappa = 1$, $\text{CONS}(E)$ denotes the resource consumption of PN, calculated as $\sum_{n_v \in N_v} \mathcal{C}(n_v) + \sum_{l_v \in L_v} (|f_L(l_v)| \times \mathcal{B}(l_v))$. Here, $|f_L(l_v)|$ quantifies the length of the physical path p_p routing the virtual link l_v. See Appendix B for the detailed problem formulation.

3. Methodology

In this section, we propose the **CON**straint-**A**ware **L**earning framework to handle complex constraints of VNE, named **CONAL**, illustrated in Figure 2. Initially, we formulate the VNE problem as a violation-tolerant CMDP, which ensures the acquisition of complete solutions and precise evaluation of solution quality and constraint violation (See the green area in Figure 2). Additionally, we present a reachability-guided optimization objective to ensure persistent constraint satisfaction while avoiding the over-conservatism of policy, which enhances both the quality and feasibility of VNE solutions. Further to address the instability of policy optimization caused by instances with no feasible solution, we propose an adaptive reachability budget method to improve the robustness of training. This method dynamically decides the value of budgets rather than a fixed zero (See the pink area in Figure 2). Furthermore, regarding the feature extractor, we propose a constraint-aware graph representation method to finely perceive the complex constraints of VNE. Concretely, we construct a heterogeneous graph to model the cross-graph status between VN and PN. We also devise several augmentations that preserve solution feasibility while enhancing the model's sensitivity of bandwidth-constrained path connectivity through contrastive learning (See the orange area in Figure 2). Overall, we build the policy with the constraint-aware graph representation method and train it with an actor-critic-based RL algorithm to achieve the reachability-guided optimization objective, where the adaptive reachability budget improves the training stability. We provide the description of both CONAL's training and inference process in Algorithm 1 and 2, placed in Appendix E.

3.1. Violation-tolerant CMDP Formulation.

To optimize resource utilization while guaranteeing solution's feasibility, we formulate solution construction of each VNE instance as a CMDP (Altman, 2021). However, VNE's hard constraints make constructing complete solutions difficult, hampering the precise assessment of solution quality and constraint violations. Thus, we propose a violation-tolerant mapping method to ensure complete solution construction and a measurement function to evaluate violations.

CMDP for VNE Solving. We consider each decision as identifying a proper physical node n_p for each virtual node n_v until all virtual nodes of VN are placed. Like existing works (Yan et al., 2020; Zhang et al., 2022; 2024b), due to the large combinatorial space of link mapping process, we incorporate link mapping into the state transitions, i.e., routing *prepared incident links* $\delta'(n_v)$ of virtual node n_v.

Definition 3.1 (Prepared incident links of virtual node)**.** Let $\mathcal{N}_v^t$ denote the set of virtual nodes that have already been placed, and n_v^t denote the to-be-placed virtual node at decision timestep t. We define $\delta(n_v^t)$ as the set of virtual links incident to n_v^t. For each virtual link $l_v \in \delta(n_v^t)$, if the link's opposite endpoint n_v' is already placed, i.e., $n_v' \in \mathcal{N}_v^t$, then we include l_v in a subset $\delta'(n_v^t)$. The subset $\delta'(n_v^t)$ consists of what we term as the prepared incident links of the virtual node n_v^t. These links are considered prepared because, upon the placement of n_v^t, both endpoints of each link in $\delta'(n_v^t)$ are placed, necessitating the routing of these links. See Appendix D.1 for an illustrative example.

We formulate this sequential decision process as a CMDP, $M = \langle S, A, R, H, C, P, \gamma \rangle$, where S denotes the state space. Each state s ($s \in S$) consists of the real-time embedding status of VN and PN. A denotes the action space, i.e., the set of physical nodes. $P : S \times A \to S$ is a state transition function. For an action $a_t = n_p^t$ to host the current be-placed virtual node n_v^t, the environment will execute the node placing and link routing. n_v^t is embeded into the n_p^t, and the available resources of n_p^t are updated accordingly. Then, for the *prepared incident links* $\delta'(n_v^t)$ of virtual nodes n_v^t, we utilize the k-shortest path algorithm to find physical paths to route them one by one. $R : S \times A \to \mathbb{R}$ is a reward function defined as follows. If the solution is completely constructed, we return its R2C metric as the reward; for the intermediate steps, we set the reward to 0. $H : S \to \mathbb{R}$ is a violation function that measures violations of constraints. We separately consider computing and bandwidth constraint violations in node placement and link routing, denoted H_N and H_L, respectively. We define $H(s) = \max(H_N(s), H_L(s))$ and allow it negative, which indicates keeping distance from nodes or links with insufficient resources. $C : S \to \mathbb{R}^+$ is a cost function calculated as $C(s) = \max(H(s), 0)$. $\gamma : S \times A \times S \to [0, 1)$ is a discount factor that balances immediate and future rewards. Next, we describe the violation-tolerant mapping method used in state transition, and explain the violation measurement functions tailored for H and C.

Violation-tolerant Mapping and Violation Measurement. Any violations of VNE constraints result in incomplete allocation, which hinders the ability to estimate the final R2C metric and constraint violation degree of infeasible solu-

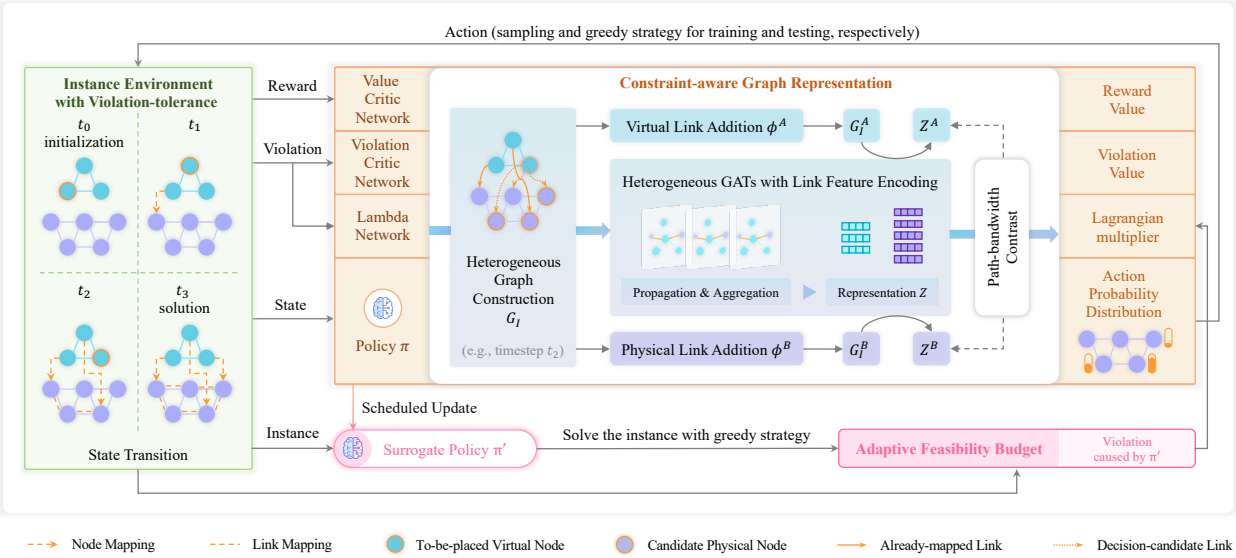

Figure 2: Overview of the proposed CONAL framework.

tions. To address this issue, we consider violation tolerance for both the node mapping and link mapping processes. This tolerance enables us to execute sustainable resource allocation of VNE, despite encountering constraint violations. Concretely, at the decision timestep t for placing the virtual node n_v^t, we generates the action probability distribution $\pi(\cdot \mid s_t)$ based on state s_t. If there are physical nodes with insufficient computing resources, we apply a mask vector that replaces the selection probability of these physical nodes that have insufficient node resources with 0 to avoid unnecessary constraint violations; but if all physical nodes are computing resource-insufficient, we also do not modify the action probability distribution; otherwise, we do nothing. Then, an action a_t (a physical node n_p^t) is selected from this distribution. we calculate the computing resource violations as $h_N^t = H_N(s_{t+1}) = \mathcal{C}(n_v^t) - \mathcal{C}(n_p^t)$.

Subsequently, we route all *prepared incident links* $\delta'(n_v^t)$ of virtual node n_v^t sequentially. For each virtual link $l_v \in \delta'(n_v^t)$, we use the k-shortest path algorithm to find a set of physical paths. If there are available paths that do not violate constraints, we select the shortest one that consumes the least resources. In this case, we consider the violation as $H_L(l_v) = \max_{l_p \in f_L(l_v)}(\mathcal{B}(l_v) - \mathcal{B}(l_p))$. However, if all paths violate constraints, we calculate the extent of the constraint violation for each path. The path with the least amount of violation is then selected to route the virtual link, whose violation is calculated by $H_L(l_v) = \sum_{l_p \in f_L(l_v)}(\mathcal{B}(l_v) - \mathcal{B}(l_p))$. After $\delta'(n_v^t)$ are routed, we define the bandwidth violations as $h_L^t = H_L(s_{t+1}) = \max_{l_v \in \delta'(n_v^t)} H_L(l_v)$. During training, we always set the solution feasibility flag $\varkappa$ to 1 to measure the final R2C metric until the solution is complete.

3.2. Reachability-guided Optimization with Adaptive Budget

Standard CMDPs focus on optimizing discounted cumulative costs to meet long-term safety, which fails to meet the consistent satisfaction requirements of VNE in all states (Liu et al., 2021). To guarantee the solution feasibility of VNE, we consider reachability analysis into CMDP to achieve state-wise zero-violation optimization (Yu et al., 2022). This objective significantly expands the feasible set of policies and mitigates the conservativeness of the policy. Additionally, to enhance the stability of policy optimization, we propose a novel adaptive reachability budget method that dynamically decides budgets, rather than always zero budget for unsolvable instances. For policy training, we adopt the Lagrange version of the PPO algorithm (Ray et al., 2019).

Reachability-guided Optimization Objective (REACH). In each decision timestep t, based on state s_t, we play an action $a_t \sim \pi(\cdot|s_t)$. Then, the network system transits into the next state according to $s_{t+1} \sim P(s_t, a_t)$, and feedback a reward $r_t = R(a_t, s_t)$, a violation $h_t = H(s_{t+1})$ and a cost $c_t = C(s_{t+1})$. In each episode, we collect all sampled states and actions with a trajectory memory $\tau = (s_o, a_0, s_1, a_1, \cdots)$. Due to hard constraints of VNE, we should achieve state-wise zero violations to ensure the solution's feasibility. An intuitive way is to maximize the expected cumulative rewards $J_r(\pi) = \mathbb{E}_{\tau\sim\pi}[\sum_t \gamma^t R(s_t, a_t))]$, while restricting expected cumulative costs $J_c(\pi) = \mathbb{E}_{\tau\sim\pi}[\sum_t \gamma^t C(s_t)]$ below zero at each decision state, i.e., $\max_\pi \mathbb{E}_{\tau\sim\pi}\left[J_r(\pi)\right]$, s.t. $\mathbb{E}_{\tau\sim\pi}\left[J_c(\pi)\right] \leq 0$. Existing safe RL methods learn the state and cost value functions, $V_r^\pi(s)$ and $V_c^\pi(s)$, that estimate the cumulative rewards and costs from state s, to solve this problem as follows.

$$\max_{\pi} \mathbb{E}_s \left[V_r^{\pi}(s)\right], \text{s.t. } \mathbb{E}_s \left[V_c^{\pi}(s)\right] \leq 0, \tag{2}$$

However, since the non-negativity of C, the optimization focuses on constraint satisfaction rather than reward maximization, causing a highly conservative policy. Thus, we consider the Hamilton-Jacobi (HJ) reachability analysis (Bansal et al., 2017) into the CMDP to obtain a policy with the best possible performance and least violations, improving both quality and feasibility of VNE solutions. We need the following concepts to present our optimization further.

Definition 3.2 (Feasible value function)**.** The feasible value function of a specific policy π measures the worst long-term constraint violation, defined as $V_h^{\pi}(s) \triangleq \max_{t\in\mathbb{N}} H\left(s_t \mid s_0 = s\right)$. Through optimizing π, the optimal feasible state-value function can achieve the least violation of the constraints, which is defined as $V_h^{\star}(s) \triangleq \min_{\pi} \max_{t\in\mathbb{N}} H\left(s_t \mid s_0 = s\right)$.

Definition 3.3 (Feasible region)**.** The feasible region S_f consists of all feasible states, where at least one policy satisfies the hard constraint, defined as $S_f \triangleq \{s \in S \mid V_h^{\star}(s) \leq 0\}$. The feasible region of a specific policy π can be defined as $\mathcal{S}_f \triangleq \{s \in S \mid V_h^{\pi}(s) \leq 0\}$.

The feasible value function $V_h^{\pi}(s)$ measures the most serious constraint violation of state s on the trajectory obtained by π. Specifically, if $V_h^{\pi}(s) \leq 0$, we have $\forall s_t, t \in \mathbb{N}, h\left(s_t\right) \leq 0$, i.e., starting from the state s, all the states are feasible on this trajectory and the policy π can satisfy the hard constraints. Otherwise, $V_h^{\pi}(s) > 0$ indicates π may violate constraints in the future states. We call $V_h^{\pi}(s) \leq 0$ the reachability constraint, ensuring that the π is inside the feasible set since the state constraint could be persistently satisfied. For the VNE problem, we aim to maximize the cumulative rewards while satisfying reachability constraints to ensure persistent zero violations, formulated as,

$$\begin{aligned} \max_{\pi} \quad & \mathbb{E}_s\Big[V_r^{\pi}(s)\,\mathbb{I}_{s\in\mathcal{S}_f} \;-\; V_h^{\pi}(s)\,\mathbb{I}_{s\notin\mathcal{S}_f}\Big], \\ \text{s.t.} \quad & \mathbb{E}_s\big[V_h^{\pi}(s)\big] \;\leq\; 0, \quad \forall s \in \mathcal{S}_f, \end{aligned} \tag{3}$$

where $\mathbb{I}$ is the indicator function. Compared to the problem (2), our reachability-guided optimization problem (3) finds the largest feasible sets, bringing less conservativeness and better performance. To solve the problem (3), we reformulate it in the Lagrangian version as follows:

$$\min_{\lambda} \max_{\pi} \mathbb{E}_s\Big[V_r^{\pi}(s)\cdot\mathbb{I}_{s\in\mathcal{S}_f} - V_h^{\pi}(s)\cdot\mathbb{I}_{s\notin\mathcal{S}_f} + \lambda V_h^{\pi}(s)\cdot\mathbb{I}_{s\in\mathcal{S}_f}\Big] \tag{4}$$

Adaptive Reachability Budget (ARB). During training, it is hard to avoid the existence of some *unsolvable VNE instances* without any feasible solution, whose all states are infeasible, i.e., $\forall s, s \notin S_f$. For example, incoming VN requires excessive resources that surpass the resource availability of PN. Judging the solvability of an instance in an NP-hard problem is a time-consuming task, which makes it difficult to distinguish between two types of states: $s \in S_f$ and $s \notin S_f$. In this case, training with samples related to these *unsolvable instances*, due to violating the Karush-Kuhn-Tucker conditions, the Lagrange multiplier may become large and even converge to infinity.

Proposition 3.4. *During online training, if there exists an instance without any feasible solution (i.e. $H(s) > 0, \forall s \in S$), then the Lagrange multiplier can become infinite.*

For its proof see Appendix D.2. The fluctuation of λ induces instability in policy optimization. This instability arises from significant shifts in the optimization focus, alternating between maximizing rewards and satisfying constraints. To address this challenge, we propose an adaptive reachability budget method to improve the stability of training, which determines an appropriate reachability budget for each VNE instance. To avoid the impractical determination of the solvability of each instance, we relax the zero-violation of reachability constraints with a dynamic reachability budget based on the instance solvability. Specifically, we employ a surrogate policy π' derived from the main policy π, and synchronize its parameters at specified steps, i.e., $\pi' \leftarrow \pi$. During the training process, both the main policy π and the surrogate policy π' attempt to solve the same incoming instance I. π uses the sampling decoding strategy for exploration to generate the trajectory $\tau \sim \pi$, while π' employs the greedy decoding strategy for prioritizing constraint satisfaction to produce the trajectory $\tau' \sim \pi'$. The max cost in τ' caused by the surrogate policy π' is considered for estimating the reachability budget $D_h^{\pi'}(s)$ for all states $s \in \tau$ sampled by policy π, formulated as follows:

$$\forall s \in \tau, D_h^{\pi'}(s) = \max_{s'\in\tau'} C(s'). \tag{5}$$

During the training process, we update the surrogate policy $\pi' \leftarrow \pi$ over multiple iterations. With the reachability guidance of π', the main policy π gradually improves constraint-aware decision-making, enhancing the training stability. Through this iterative learning, both policies π and π' achieve better constraint satisfaction while maintaining exploring for better solutions. Finally, we obtain the refined Lagrangian objective with adaptive reachability budget:

$$\min_{\lambda} \max_{\pi} \mathbb{E}_s \left[V_r^{\pi}(s) - \lambda\left(V_h^{\pi}(s) - D_h^{\pi'}(s)\right)\right]. \tag{6}$$

Here, considering the varying extent of violation in different states, we introduce a neural lambda network $\lambda = \Lambda(s)$ to dynamically adjust Lagrangian multipliers during training, similar to Ma et al. (2021). To optimize the policy, we leverage the actor-critic framework with Proximal Policy Optimization (PPO) as the training algorithm (Ray et al., 2019), similar to works (Yu et al., 2022; Ma et al., 2021). See Appendix D.5 for the details of this training method. Next, we will introduce our proposed constraint-aware graph networks used as the feature encoder of policy.

3.3. Constraint-aware Graph Representation

The VNE processing is governed by complex and multi-faceted constraints, presenting challenges in representation learning. These include the interaction of cross-graph status and the assessment of bandwidth-constrained path connectivity. To address this issue, we propose a constraint-aware graph representation method with a heterogeneous modeling module for cross-graph status fusion, and a contrastive learning-based module to enhance path connectivity awareness. It efficiently perceives the complex constraints of VNE, providing a higher guarantee of solution feasibility.

Heterogeneous Modeling (HM). Instead of separate feature extraction of VN G_v and PN G_p, we integrate them into a heterogeneous graph G_I by introducing several hypothetical cross-graph links. G_I comprises two distinct node types: virtual and physical nodes, and we denote their attributes as X_v^n and X_p^n. These node attributes include computing resource demands or availability, link counts, and the aggregated bandwidth characteristics (maximum, minimum, and average) of adjacent links. Similarly, there are two link types: virtual and physical links, whose attributes are link bandwidth demands or availability. We denote these link attributes as X_v^l and X_p^l, respectively. Additionally, we introduce specialized heterogeneous links to capture the current embedding state: already-mapped links, which connect virtual nodes to their hosting physical nodes, and imaginary decision links, which connect the current yet-to-be-decided virtual node with all *potential physical nodes*. Here, *potential physical node* refers to one that hosts no virtual nodes and has enough computing resources available. We group these heterogeneous links into sets $L_{v,p,m}$ for already-mapped links and $L_{v,p,d}$ for decision-candidate links. We uniformly set these two types of links' attributes to 1, denoted as $X_{v,p,m}^l$ and $X_{v,p,d}^l$, respectively. To encode this graph's topological and attribute information, we enhanced widely-used graph attention networks (GAT) (Veličković et al., 2018) by integrating heterogeneous link fusion and link attribute encoding in the propagation process. See Appendix D.3 for its details. Inputting the heterogeneous graph's features into this network, we obtain the final node representations $Z = \{Z_v, Z_p\}$, where Z_v and Z_p denote physical and virtual node representations.

Path-bandwidth Contrast (PC). Bandwidth constraints of VNE significantly impact solution feasibility, particularly in the context of path routing complexity. At each decision timestep, we need to carefully select a physical node n_p^t for placing the current virtual node n_v^t. This selection is dominated by ensuring that feasible connective paths exist to all other physical nodes hosting the virtual node's neighbors. Here, the feasibility of the path is dominated by the bandwidth availability of physical links to support the bandwidth requirements of all *prepared incident links* $\delta'(n_v^t)$. GNNs build up on the propagation mechanism along links to increase awareness of the topology information. However, not all physical links contribute positively to this awareness; some with insufficient bandwidths may even introduce noise into node representations. This emphasizes the necessity to integrate bandwidth constraint awareness within GNNs to perceive the path feasibility.

To address this challenge, we propose a novel path-bandwidth contrast method to enhance bandwidth constraint awareness via contrastive learning, whose core idea is creating augmented views with feasibility-consistency augmentations and making node representations in these views close.

Definition 3.5 (Feasibility-consistency Augmentations)**.** Let Φ denote a set of augmentation methods and $\mathcal{F}$ denote the function indicating the feasibility of solutions. Given any VNE instance I and a solution $E = f_G(I)$, we have $\mathcal{F}(E) = \mathcal{F}(\phi(E)), \forall I \in \mathcal{I}, \phi \in \Phi$.

These augmentations generate multiple views of the original heterogeneous graph, which maintain the same feasibility semantics before and after their application. Following this principle, we develop several augmentation methods by modifying the topology of either VN or PN without impacting solution feasibility. (a) *Physical Link Addition* ϕ^A. We add a specific number $\epsilon \cdot |N^p|$ of physical links in PN, whose bandwidth resources are equal to the difference between the smallest requirements among all virtual links and 1, i.e., $\min_{l_v \in L_v} \mathcal{B}(l_v) - 1$. (b) *Virtual Link Addition* ϕ^B. We add a specific number $\epsilon \cdot |N^v|$ of virtual links that require a zero bandwidth resource to enhance the complexity and connectivity of the VN. Here, ϵ is an augment ratio that determines the proportion of links to be added based on the number of nodes in the network.

After applying these augmentations, we create two new views $G_I^A = \phi_A(G_I)$ and $G_I^B = \phi^B(G_I)$, which have same feasibility semantics of VNE instance I. Using our heterogeneous graph network, we extract node representations under views G_I^A and G_I^B, denoted as Z^A and Z^B, respectively. Subsequently, we utilize contrastive learning to enhance the proximity of node representations under the augmented views G_I^A and G_I^B. This necessitates that the model precisely discerns the noisy implications of those links with less bandwidth that play no impact on solution feasibility. Through this method, we aim to enhance the model's sensitivity towards link bandwidth, effectively mitigate the influence of irrelevant links in the GNN propagation process, and bolster its overall awareness of bandwidth constraints. In this work, we adopt the Barlow Twins method (Zbontar et al., 2021) for its simplicity and effectiveness, which circumvents negative sample selection and maintains the original network architecture. Given the embeddings under two augmented views, H^a and H^b, we use this contrastive loss L_{CL} to reduce redundancy between embedding components by aligning their cross-correlation matrix with the identity matrix. This unsupervised loss can be seamlessly integrated into the training process of RL. See Appendix D.4

for the details of Barlow Twins method.

3.4. Computational Complexity Analysis

Note that CONAL solely uses its surrogate policy and path-bandwidth contrast module for policy optimization during training. During inference, CONAL has a computational complexity of $O\left(|N_v| \cdot K \cdot \left(|L_p|d + |N_p + N_v|d^2\right)\right)$. See Appendix D.6 for detailed explanations.

4. Experiments

To evaluate the effectiveness of CONAL, we compare it with state-of-the-art baselines in various network scenarios.

4.1. Experimental Settings

Simulation Configurations. Similar to most previous works (Geng et al., 2023; Yan et al., 2020), we evaluate CONAL in *Virne* benchmarks that simulate various network systems (See Appenidx H for its introduction). We adopt a widely-used Waxman topology with 100 nodes and nearly 500 links (Waxman, 1988) as the physical network, named **WX100**. Computing resources of physical nodes and bandwidth resources of physical links are uniformly distributed within the range of [50, 100] units. In default settings, for each simulation run, we create 1000 VN with varying sizes from 2 to 10. The computing resource demands of the nodes and the bandwidth requirements of the links within each VN are uniformly distributed within the range of [0, 20] and [0, 50] units, respectively. The virtual nodes in each VN are randomly interconnected with a probability of 50%. The lifetime of each VN follows an exponential distribution with an average of 500 time units. The arrival of these VNs follows a Poisson process with an average rate η, where η denotes the average arrived VN count per unit of time. In the subsequent experiments, we manipulate the distribution settings of VNs and change the PN topologies to simulate various network systems.

Implementation Settings. We describe the details of CONAL implementations, simulation for training and testing, and computer resources in Appendix F.1. Notably, in scenarios where the PN topology remains unchanged, we employ the pre-trained models developed under default settings to investigate the adaptability and generalization across diverse conditions in network systems.

Compared Baselines. We compare CONAL with both heuristic and RL-based methods. The heuristic baselines includes node ranking-based methods (i.e., NRM-VNE (Zhang et al., 2018), GRC-VNE (Gong et al., 2014), NEA-VNE (Fan et al., 2023)) and meta-heuristics (i.e., GA-VNE (Zhang et al., 2019), PSO-VNE (Jiang & Zhang, 2021)). The learning-based baselines are PG-CNN (Ma et al., 2023), DDPG-ATT (He et al., 2023a), A3C-GCN (Zhang et al., 2024b), and GAL-VNE (Geng et al., 2023). See Appendix F.2 for their descriptions.

Evaluation Metrics. Following most previous research (Fischer et al., 2013; Yan et al., 2020), we adopt widely used key metrics for VNE algorithm evaluation: VN Acceptance Rate (**VN_ACR**); Long-Term REVenue (**LT_REV**); Long-Term Revenue-to-Consumption ratio (**LT_R2C**). We also consider **AV**era**G**e Solving Time (**AVG_ST**) as an additional metric to measure the computational efficiency, due to the real-time demands of online network systems. Additionally, for CONAL and its variations, we employ Constraint VIOlation (**C_VIO**) to measure the degree of constraint satisfaction. See Appendix F.4 for their definitions.

4.2. Results and Analysis

Overall Evaluation. The results of VNE algorithms under default settings are shown in Table 1. We observe that CONAL outperforms baselines across three key performance metrics. This is due to CONAL's ability to effectively perceive and handle the complex constraints of VNE. Among baselines, NEA-VNE, GA-VNE, and GAL-VNE are the best node-ranking-based heuristics, meta-heuristics, and RL-based methods. However, GA-VNE which relies on extensive search in the solution space has a longer running time, while GAL-VNE exhibits lower R2C metrics. Compared to NEA-VNE, GA-VNE and GAL-VNE, CONAL achieves improvements of (10.04%, 11.07%, 13.99%), (10.61%, 28.72%, 17.80%) and (4.77%, 24.04%, 6.21%) in term of (VN_ACR, LT_R2C, and LT_REV), respectively. We also observe that CONAL outperforms all RL-based baselines across key performance metrics, demonstrating the superiority of its modeling, optimization, and representation methods. Although CONAL's running time is not the lowest, it remains competitive, comparable to NEA-VNE and A3C-GCN, and outperforms other baselines such as GA-VNE and MCTS-VNE. These results underscore that CONAL provides high-quality and feasible solutions to improve resource utilization and request acceptance.

Ablation Study. We design several variations to manifest the efficacy of each proposed component: $\text{CONAL}_{\text{w/o HM}}$, $_{\text{w/o PC}}$, $_{\text{w/o HM \& PC}}$, $_{\text{w/o REACH}}$, and $_{\text{w/o ARB}}$. See Appendix F.3 for their descriptions. The results are presented in Table 1. Compared to the first three variants, CONAL achieves superior results across various performance metrics. This indicates that our constraint-aware graph representation method enhances the constraint awareness of policy. Notably, $\text{CONAL}_{\text{w/o PC}}$ shows the most significant performance declines, even worse than $\text{CONAL}_{\text{w/o HM \& PC}}$. This may be due to heterogeneous graph modeling methods increasing the link complexity of graph, which highlights the necessity for improving bandwidth constraint sensitivity. Furthermore, $\text{CONAL}_{\text{w/o REACH}}$ and $\text{CONAL}_{\text{w/o ARB}}$ also decrease performance, which demonstrates that our optimization method facilitates both resource utilization and constraint satisfaction. This study shows that each component of CONAL contributes to its overall performance, enhancing its ability to handle and perceive the complex constraints of VNE.

Table 1: Results in overall evaluation and ablation study. Each value consists of the mean and standard error.

	VN_RAC ↑	LT_R2C ↑	LT_REV ($\times 10^7$) ↑	C_VIO ($\times 10^3$) ↓	AVG_ST ($\times 10^{-1}$ s) ↓
NRM-VNE	0.675 ± 0.011	0.461 ± 0.003	7.649 ± 0.089	-	$\mathbf{1.285 \pm 0.042}$
GRC-VNE	0.694 ± 0.020	0.468 ± 0.004	7.888 ± 0.081	-	2.737 ± 0.056
NEA-VNE	0.732 ± 0.017	0.558 ± 0.007	8.635 ± 0.183	-	4.471 ± 0.656
GA-VNE	0.735 ± 0.043	0.477 ± 0.007	8.355 ± 0.082	-	47.462 ± 1.117
PSO-VNE	0.723 ± 0.025	0.456 ± 0.004	7.854 ± 0.060	-	51.955 ± 3.512
MCTS-VNE	0.700 ± 0.085	0.477 ± 0.006	7.809 ± 0.394	-	15.512 ± 8.096
PG-CNN	0.682 ± 0.020	0.487 ± 0.004	7.523 ± 0.156	-	3.906 ± 0.057
DDPG-ATT	0.707 ± 0.021	0.469 ± 0.003	7.961 ± 0.091	-	2.991 ± 0.054
A3C-GCN	0.743 ± 0.019	0.540 ± 0.006	8.814 ± 0.223	-	3.585 ± 0.200
GAL-VNE	0.776 ± 0.014	0.495 ± 0.003	9.267 ± 0.162	-	6.881 ± 0.785
$\text{CONAL}_{\text{w/o HM}}$	0.804 ± 0.044	0.584 ± 0.004	9.597 ± 0.107	3.410 ± 0.080	3.754 ± 0.124
$\text{CONAL}_{\text{w/o PC}}$	0.735 ± 0.036	0.573 ± 0.002	8.407 ± 0.128	5.960 ± 0.068	4.117 ± 0.273
$\text{CONAL}_{\text{w/o HM \& PC}}$	0.789 ± 0.058	0.585 ± 0.006	9.446 ± 0.084	4.053 ± 0.072	3.909 ± 0.104
$\text{CONAL}_{\text{w/o REACH}}$	0.792 ± 0.049	0.611 ± 0.007	9.607 ± 0.073	3.954 ± 0.045	4.052 ± 0.069
$\text{CONAL}_{\text{w/o ARB}}$	0.806 ± 0.034	0.596 ± 0.003	9.639 ± 0.065	3.656 ± 0.087	4.074 ± 0.093
CONAL	$\mathbf{0.813 \pm 0.042}$	$\mathbf{0.614 \pm 0.006}$	$\mathbf{9.842 \pm 0.091}$	$\mathbf{2.773 \pm 0.083}$	4.180 ± 0.104

Training Stability Study. (A) *Training Conditions vs. Testing Performance*. We first explore the impact of training conditions on testing performance. Results in Figure 4 show CONAL maintains a more stable testing performance compared to $\text{CONAL}_{\text{w/o ARB}}$. (B) *Convergence Analysis*. We also compare their training convergence curves of reward and Lagrange multiplier λ in Figure 5, where CONAL converges to a higher reward and has a stably small λ. These findings are attributed to the efficient handling of insolvable instances by our ARB module. See Appendix G.1 for details

Generalizability Study. Practical network systems face fluctuations in traffic patterns and resource demands due to dynamic user service requirements. To study generalizability, we test trained models in various network conditions. (A) *Request Frequency Sensitivity Study.* We assess the sensitivity of CONAL to varying arrival rates of VN requests by adjusting the average request frequency η. Results illustrated in Figure 6 highlight CONAL's effectiveness in handling network scenarios with fluctuating request rates, even as competition for resources increases. (B) *Dynamic Request Distribution Study.* We simulate varying network conditions by modifying resource demands and node sizes of VN requests in different stages. Results in Figure 7 show that CONAL can generalize effectively in dynamic systems with shifting requirements. See Appendix G.2 for details.

Scalability Analysis. To assess the scalability of CONAL, we explore its performance in large-scale network systems and its time consumption to adapt to varying network sizes. In summary: (A) *Large-scale Network Validation*. We evaluate CONAL on a Waxman topology with 500 nodes representing a large-scale cloud cluster. The results demonstrate that CONAL consistently outperforms all baseline models, even in large-scale network systems. (B) *Solving Time Scale Analysis*. We increase the size of physical network from 200 to 1,000 nodes to simulate network systems of varying scales. The results show that even at larger network scales, CONAL maintains efficient solving times while delivering excellent performance. See Appendix G.3 for details.

Real-world Network Topology Validation. To verify the effectiveness of CONAL in real-world network systems, we conduct experiments on two well-known networks (Yan et al., 2020; He et al., 2023a): GEANT and BRAIN. The results shown in Table 3 reveal that CONAL outperforms all baselines across both network systems on performance, which shows the effectiveness of CONAL in practical systems and various topologies. See Appendix G.4 for details.

Extension to Latency-aware VNE. We further study the VNE variation in edge computing with latency consideration, which additionally introduces such constraint. Results in Table 4 show that CONAL exhibits superior performance which efficiently handles complex multi-type constraints in this variation of VNE. See Appendix G.5 for details.

5. Conclusion

In this paper, we proposed the CONAL for VNE to enhance constraint management and training stability, which is critical to the performance and reliability of network systems. Specifically, we formulated the VNE problem as a violation-tolerant CMDP to optimize both the quality and feasibility of solutions, which precisely evaluates the quality and violation of the solution. Additionally, we presented a reachability-guided optimization objective with an adaptive feasibility budget method to ensure persistent constraint satisfaction while alleviating the conservativeness of policy. This approach also addresses the instability of policy optimization caused by unsolvable instances. Furthermore, to finely perceive the complex constraints of VNE, we proposed a constraint-aware graph representation method, consisting of a heterogeneous modeling module and a path-bandwidth contrast module. Finally, we conducted extensive experiments to verify the effectiveness of CONAL.

Impact Statements

This paper presents work whose goal is to advance the field of Machine Learning for Combinatorial Optimization and Networking Resource Allocation. There are many potential societal consequences of our work, none which we feel must be specifically highlighted here.

References

Achiam, J., Held, D., Tamar, A., and Abbeel, P. Constrained policy optimization. In *International conference on machine learning*, pp. 22–31. PMLR, 2017.

Adoga, H. U. and Pezaros, D. P. Towards latency-aware vnf placement on heterogeneous hosts at the network edge. In *IEEE Global Communications Conference*, pp. 6383–6388, 2023.

Altman, E. *Constrained Markov decision processes*. Routledge, 2021.

Bansal, S., Chen, M., Herbert, S., and Tomlin, C. J. Hamilton-jacobi reachability: A brief overview and recent advances. In *2017 IEEE 56th Annual Conference on Decision and Control (CDC)*, pp. 2242–2253. IEEE, 2017.

Bengio, Y., Lodi, A., and Prouvost, A. Machine learning for combinatorial optimization: a methodological tour d'horizon. *European Journal of Operational Research*, 290(2):405–421, 2021.

Bi, J., Ma, Y., Zhou, J., Song, W., Cao, Z., Wu, Y., and Zhang, J. Learning to handle complex constraints for vehicle routing problems. In *Neural Information Processing Systems*, 2024.

Chen, T., Kornblith, S., Norouzi, M., and Hinton, G. A simple framework for contrastive learning of visual representations. In *International conference on machine learning*, pp. 1597–1607, 2020.

Chowdhury, N. M. M. K., Rahman, M. R., and Boutaba, R. Virtual network embedding with coordinated node and link mapping. In *IEEE International Conference on Computer Communications*, pp. 783–791, 2009.

Dehury, C. K. and Sahoo, P. K. DYVINE: Fitness-based dynamic virtual network embedding in cloud computing. *IEEE Journal on Selected Areas in Communications*, 37 (5):1029–1045, 2019.

Fan, W., Xiao, F., Lv, M., Han, L., Wang, J., and He, X. Node essentiality assessment and distributed collaborative virtual network embedding in datacenters. *IEEE Transactions on Parallel and Distributed Systems*, 34(4): 1265–1280, 2023.

Fischer, A., Botero, J. F., Beck, M. T., de Meer, H., and Hesselbach, X. Virtual network embedding: A survey. *IEEE Communications Surveys Tutorials*, 15(4):1888–1906, 2013.

Geng, H., Wang, R., Wu, F., and Yan, J. Gal-vne: Solving the vne problem with global reinforcement learning and local one-shot neural prediction. In *Proceedings of the 29th ACM SIGKDD Conference on Knowledge Discovery and Data Mining*, pp. 531–543, 2023.

Gong, L., Wen, Y., Zhu, Z., and Lee, T. Toward profit-seeking virtual network embedding algorithm via global resource capacity. In *IEEE International Conference on Computer Communications*, pp. 1–9, 2014.

Grill, J.-B., Strub, F., Altché, F., Tallec, C., Richemond, P., Buchatskaya, E., Doersch, C., Avila Pires, B., Guo, Z., Gheshlaghi Azar, M., et al. Bootstrap your own latent-a new approach to self-supervised learning. *Advances in neural information processing systems*, 33:21271–21284, 2020.

Gu, S., Yang, L., Du, Y., Chen, G., Walter, F., Wang, J., Yang, Y., and Knoll, A. A review of safe reinforcement learning: Methods, theory and applications. *arXiv preprint arXiv:2205.10330*, 2022.

Haeri, S. and Trajković, L. Virtual network embedding via Monte Carlo tree search. *IEEE Transactions on Cybernetics*, 48(2):510–521, 2017.

He, N., Yang, S., Li, F., Trajanovski, S., Zhu, L., Wang, Y., and Fu, X. Leveraging deep reinforcement learning with attention mechanism for virtual network function placement and routing. *IEEE Transactions on Parallel and Distributed Systems*, 34(4):1186–1201, 2023a.

He, T., Zhao, W., and Liu, C. Autocost: Evolving intrinsic cost for zero-violation reinforcement learning. In *Proceedings of the AAAI Conference on Artificial Intelligence*, volume 37, pp. 14847–14855, 2023b.

Jiang, C. and Zhang, P. *VNE-HPSO Virtual Network Embedding Algorithm Based on Hybrid Particle Swarm Optimization*, pp. 129–152. Springer Singapore, Singapore, 2021.

Jin, P., Fei, X., Zhang, Q., Liu, F., and Li, B. Latency-aware vnf chain deployment with efficient resource reuse at network edge. In *IEEE Conference on Computer Communications*, pp. 267–276, 2020.

Kingma, D. P. and Ba, J. Adam: A method for stochastic optimization. *arXiv preprint arXiv:1412.6980*, 2014.

Liu, Y., Halev, A., and Liu, X. Policy learning with constraints in model-free reinforcement learning: A survey.

In *The 30th International Joint Conference on Artificial Intelligence (IJCAI)*, 2021.

Ma, H., Guan, Y., Li, S. E., Zhang, X., Zheng, S., and Chen, J. Feasible actor-critic: Constrained reinforcement learning for ensuring statewise safety. *arXiv preprint arXiv:2105.10682*, 2021.

Ma, S., Yao, H., Mai, T., Yang, J., He, W., Xue, K., and Guizani, M. Graph convolutional network aided virtual network embedding for internet of thing. *IEEE Transactions on Network Science and Engineering*, 10(1):265–274, 2023.

Mazyavkina, N., Sviridov, S., Ivanov, S., and Burnaev, E. Reinforcement learning for combinatorial optimization: A survey. *Computers & Operations Research*, 134: 105400, 2021.

Oord, A. v. d., Li, Y., and Vinyals, O. Representation learning with contrastive predictive coding. *arXiv preprint arXiv:1807.03748*, 2018.

Pan, Y., Chen, Y., and Lin, F. Adjustable robust reinforcement learning for online 3d bin packing. In *Advances in Neural Information Processing Systems*, volume 36, pp. 51926–51954, 2023.

Ray, A., Achiam, J., and Amodei, D. Benchmarking safe exploration in deep reinforcement learning. *arXiv preprint arXiv:1910.01708*, 7(1):2, 2019.

Rost, M. and Schmid, S. On the hardness and inapproximability of virtual network embeddings. *IEEE/ACM Transactions on Networking*, 28(2):791–803, 2020.

Schulman, J., Wolski, F., Dhariwal, P., Radford, A., and Klimov, O. Proximal policy optimization algorithms. *arXiv preprint arXiv:1707.06347*, 2017.

Shahriar, N., Chowdhury, S. R., Ahmed, R., Khan, A., Fathi, S., Boutaba, R., Mitra, J., and Liu, L. Virtual network survivability through joint spare capacity allocation and embedding. *IEEE Journal on Selected Areas in Communications*, 36(3):502–518, 2018.

Veličković, P., Cucurull, G., Casanova, A., Romero, A., Lio, P., and Bengio, Y. Graph attention networks. In *International Conference on Learning Representations*, 2018.

Wang, T., Fan, Q., Li, X., Zhang, X., Xiong, Q., Fu, S., and Gao, M. DRL-SFCP: Adaptive service function chains placement with deep reinforcement learning. In *IEEE International Conference on Communications*, pp. 1–6, 2021.

Wang, T., Shen, L., Fan, Q., Xu, T., Liu, T., and Xiong, H. Joint admission control and resource allocation of virtual network embedding via hierarchical deep reinforcement learning. *IEEE Transactions on Services Computing*, pp. 1–14, 2023.

Wang, T., Fan, Q., Wang, C., Yang, L., Ding, L., Yuan, N. J., and Xiong, H. Flagvne: A flexible and generalizable reinforcement learning framework for network resource allocation. In *International Joint Conference on Artificial Intelligence*, 2024.

Waxman, B. Routing of multipoint connections. *IEEE Journal on Selected Areas in Communications*, 6(9):1617–1622, 1988.

Yan, Z., Ge, J., Wu, Y., Li, L., and Li, T. Automatic virtual network embedding: A deep reinforcement learning approach with graph convolutional networks. *IEEE Journal on Selected Areas in Communications*, 38(6):1040–1057, 2020.

Yang, L., Ji, J., Dai, J., Zhang, L., Zhou, B., Li, P., Yang, Y., and Pan, G. Constrained update projection approach to safe policy optimization. *Advances in Neural Information Processing Systems*, 35:9111–9124, 2022.

Yao, H., Ma, S., Wang, J., Zhang, P., Jiang, C., and Guo, S. A continuous-decision virtual network embedding scheme relying on reinforcement learning. *IEEE Transactions on Network and Service Management*, 17(2):864–875, 2020.

Ye, H., Wang, J., Cao, Z., Liang, H., and Li, Y. Deepaco: Neural-enhanced ant systems for combinatorial optimization. *Advances in Neural Information Processing Systems*, 36, 2023.

Yi, B., Wang, X., Li, K., Huang, M., et al. A comprehensive survey of network function virtualization. *Computer Networks*, 133:212–262, 2018.

Yu, D., Ma, H., Li, S., and Chen, J. Reachability constrained reinforcement learning. In *International Conference on Machine Learning*, pp. 25636–25655. PMLR, 2022.

Zbontar, J., Jing, L., Misra, I., LeCun, Y., and Deny, S. Barlow twins: Self-supervised learning via redundancy reduction. In *International conference on machine learning*, pp. 12310–12320. PMLR, 2021.

Zhang, C., Cao, Z., Song, W., Wu, Y., and Zhang, J. Deep reinforcement learning guided improvement heuristic for job shop scheduling. In *International Conference on Learning Representations*, 2024a.

Zhang, D. W., Rainone, C., Peschl, M., and Bondesan, R. Robust scheduling with gflownets. In *International Conference on Learning Representations*, 2023.

Zhang, P., Yao, H., and Liu, Y. Virtual network embedding based on computing, network, and storage resource constraints. *IEEE Internet of Things Journal*, 5(5):3298–3304, 2018.

Zhang, P., Yao, H., Li, M., and Liu, Y. Virtual network embedding based on modified genetic algorithm. *Peer-to-Peer Networking and Applications*, 12(2):481–492, 2019.

Zhang, P., Su, Y., Wang, J., Jiang, C., Hsu, C.-H., and Shen, S. Reinforcement learning assisted bandwidth aware virtual network resource allocation. *IEEE Transactions on Network and Service Management*, 19(4):4111–4123, 2022.

Zhang, X., Cui, L., Tso, F. P., Li, Z., and Jia, W. Dapper: Deploying service function chains in the programmable data plane via deep reinforcement learning. *IEEE Transactions on Services Computing*, pp. 1–14, 2024b.

Zhao, H., She, Q., Zhu, C., Yang, Y., and Xu, K. Online 3d bin packing with constrained deep reinforcement learning. In *Proceedings of the AAAI Conference on Artificial Intelligence*, volume 35, pp. 741–749, 2021.

Zhao, W., He, T., and Liu, C. Model-free safe control for zero-violation reinforcement learning. In *Proceedings of the 5th Conference on Robot Learning*, volume 164, pp. 784–793. PMLR, 2022.

Zhao, W., He, T., Chen, R., Wei, T., and Liu, C. State-wise safe reinforcement learning: A survey. In *International Joint Conference on Artificial Intelligence*, 2023.

Zhuang, W., Ye, Q., Lyu, F., Cheng, N., and Ren, J. SDN/NFV-empowered future IoV with enhanced communication, computing, and caching. *Proceedings of the IEEE*, 108(2):274–291, 2020.

Appendix

A Related Work **13**

B Problem Formulation **13**

B.1 Optimization Objectives 14

B.2 Constraint Conditions 14

C Preliminary Study **15**

D Model Details **15**

D.1 Illustrative Explanation of Prepared Incident Links 15

D.2 Proof of Lagrange Multiplier Convergence 15

D.3 Heterogeneous Graph Network 16

D.4 Barlow Twins Loss Function 16

D.5 Lagrangian-based PPO Training Method. 17

D.6 Detailed Analysis of Computational Complexity 17

E Descriptions of Training and Inference Process **18**

E.1 Training Process of CONAL 18

E.2 Inference Process of CONAL 19

F Experimental Details **19**

F.1 Implementation Details 19

F.2 Baseline Descriptions 20

F.3 Variations Descriptions 20

F.4 Metric Definitions 21

G Addtional Evaluation **22**

G.1 Training Stability Study 22

G.2 Generalizability Study 23

G.3 Scalability Analysis 25

G.4 Real-world Network Topology Validation 25

G.5 Extension to Latency-aware VNE 26

G.6 Hyperparameter Impact Study 27

H Used Benchmark and Assets **28**

A. Related Work

In this section, we discuss related work on VNE algorithms, RL for COPs, and safe RL methods.

VNE Algorithms. To solve this challenging and significant problem, many approaches have been designed for VNE, which can be classified as exact, heuristics, and learning-based methods. Initially, exact algorithms formulate the VNE problem as integer linear programming (Shahriar et al., 2018) or mixed integer linear programming (Chowdhury et al., 2009), and then solve them with exact solvers. However, this is impractical due to extensive computations and time consumption. Thus, numerous heuristic algorithms have been proposed to offer solutions within an acceptable time, such as node ranking strategies (Zhang et al., 2018; Gong et al., 2014; Fan et al., 2023), meta-heuristics (Dehury & Sahoo, 2019; Zhang et al., 2019; Jiang & Zhang, 2021), etc. However, they heavily rely on manual heuristic design and merely for specific scenarios. Recently, reinforcement learning has emerged as a promising solution for VNE and many RL-based VNE algorithms have been proposed (Haeri & Trajković, 2017; Wang et al., 2021; Zhang et al., 2022; He et al., 2023a; Zhang et al., 2024b; Geng et al., 2023; Wang et al., 2024). In general, they model the solution construction process of each VNE instance as an MDP, but do not consider the fine-grained constraint violations. Then, they leverage existing network networks (e.g., convolutional neural network, GNN, etc.) to extract features from PN and VN, separately. Finally, they optimize the model with different RL methods (e.g., asynchronous advantage actor-critic, PPO, etc.). Although they use the action masking mechanism to select physical nodes with adequate computing resources and avoid unnecessary failures, they can not address potential violations of path-level bandwidth constraints during state transitions, which still lead to numerous *failure samples* during exploration. Consequently, they struggle to handle such complex constraints of VNE thereby compromising performance, since they lack constraint awareness in MDP modeling, representation learning, and policy optimization.

RL for COPs. The application of RL to solve COPs has emerged as a hot topic in decision-making, which aims to learn efficient solving strategies from data (Bengio et al., 2021). Many efforts have been directed toward classic COPs such as routing (Ye et al., 2023; Bi et al., 2024), scheduling (Zhang et al., 2023; 2024a), bin packing (Pan et al., 2023; Zhao et al., 2021), etc. These approaches can be broadly categorized into two types based on their solving processes: construction and improvement. While improvement methods start with an initial solution and use an RL policy to iteratively refine it, construction methods build a solution incrementally from scratch (Mazyavkina et al., 2021). Construction methods typically employ RL to guide the sequential selection to form a complete solution. Given the real-time requirements of practical network systems, most existing RL-based VNE algorithms are designed as construction methods to provide solutions within an acceptable time (Zhang et al., 2022; He et al., 2023a; Zhang et al., 2024b). In contrast to these classic COPs, VNE presents unique complexities in representation learning due to its multifaceted and hard constraints, such as the interaction of cross-graph status and the assessment of bandwidth-constrained path connectivity. Furthermore, the existence of unsolvable instances in the training process can compromise robustness, potentially causing ineffective policies.

Safe RL Methods. Safe RL aims to maximize the expected rewards while ensuring safety constraints are not violated (Gu et al., 2022). Early efforts in safe RL focus on keeping cumulative constraint violations below a fixed cost budget (Achiam et al., 2017; Ray et al., 2019; Yang et al., 2022). To address the stricter constraint requirements of practical applications, recent works have proposed achieving state-wise safety, which ensures the satisfaction of instantaneous constraints at each decision timestep (Zhao et al., 2023; 2022; He et al., 2023b; Yu et al., 2022). One promising approach involves incorporating reachability analysis into the CMDP framework (Yu et al., 2022). This method employs a reachability function to assess the state feasibility, which significantly expands the feasible set of policy, and mitigates the conservativeness of the policy. However, modeling VNE as a reachability-guided CMDP presents challenges. Concretely, In the process of solution construction, if any constraints are violated, the process will be early terminated and lead to incomplete solutions. This hinders precise measurement of both the quality of solutions and the degree of constraint violations. Additionally, these methods typically assume a non-empty feasible set. But for VNE, where it is hard to avoid facing unsolvable instances without any feasible solution, these approaches often confront the challenges of unstable policy optimization, since the constraints of these instances are impossibly satisfied.

B. Problem Formulation

In this section, we provide the mathematical programming formulation of the VNE problem.

B.1. Optimization Objectives

The main goal of VNE is to make full use of the physical network resources to improve the revenue of ISPs while satisfying the service requests of users as much as possible. To address the stochastic nature of online networking, we and existing studies (Wang et al., 2021; He et al., 2023a; Zhang et al., 2024b), aim to minimize the embedding cost of each arriving VN request onto the physical network. This way enhances resource utilization and improves the VN request acceptance rate. To evaluate the quality of solution $E = f_G(I)$, we employ the widely used indicator, Revenue-to-Consumption ratio (R2C), defined as follows:

$$\text{R2C}\left(E\right) = \left(\varkappa \cdot \text{REV}\left(E\right)\right) / \text{CONS}\left(E\right). \tag{7}$$

Here, $\varkappa$ is a binary variable representing the feasibility of a solution: $\varkappa = 1$ if the solution E for the instance I is accepted, and $\varkappa = 0$ otherwise. REV(E) denotes the revenue generated by the VN request G_v and CONS(E) denotes the embedding consumption, which are computed as follows:

$$\text{REV}(E) = \sum_{n_v \in N_v} \mathcal{C}(n_v) + \sum_{l^v \in L_v} \mathcal{B}(l^v), \tag{8}$$

$$\text{CONS}(E) = \sum_{n_v \in N_v} \mathcal{C}(n_v) + \sum_{l^v \in L_v} |f_L(l_v)| \mathcal{B}(l^v), \tag{9}$$

where $|f_L(l_v)|$ denotes the hop count of the physical path $p_p = f_L(l_v)$ routing the virtual link l_v.

B.2. Constraint Conditions

The process of embedding a VN request G_v onto the physical network is represented by a mapping function $f_G : G_v \to G_p$. In this process, we need to decide two types of boolean variables: (1) $x_i^m = 1$ if virtual node n_v^m is placed in physical node n_p^i, and 0 otherwise; (2) $y_{i,j}^{m,w} = 1$ if virtual link $l_{m,w}^v = (n_v^m, n_v^w)$ traverses physical link $l_{i,j}^p = (n_p^i, n_p^j)$, and 0 otherwise. Here, m and w are identifiers for virtual nodes, while i and j are identifiers for physical nodes. A VN request is successfully embedded if a feasible mapping solution is found, satisfying the following constraints:

$$\sum_{n_p^i \in n_p} x_i^m = 1, \forall n_v^m \in n_v, \tag{10}$$

$$\sum_{n_v^m \in N_v} x_i^m \leq 1, \forall n_p^i \in N_p, \tag{11}$$

$$x_i^m \mathcal{C}(n_v^m) \leq \mathcal{C}(n_p^i), \forall n_v^m \in N_v, n_p^i \in N_p, \tag{12}$$

$$\sum_{n_p^i \in \Omega(n_p^k)} y_{i,k}^{m,w} - \sum_{n_p^j \in \Omega(n_p^k)} y_{k,j}^{m,w} = x_k^m - x_k^w, \forall l_{m,w}^v \in L_v, n_v^k \in N_p, \tag{13}$$

$$y_{i,j}^{m,w} + y_{j,w}^{m,w} \leq 1, \forall l_{m,w}^v \in L_v, l_{i,j}^p \in L_p, \tag{14}$$

$$\sum_{l_{m,w}^v \in L_v} (y_{i,j}^{m,w} + y_{j,i}^{m,w}) \mathcal{B}(l_{m,w}^v) \leq \mathcal{B}((l_{i,j}^p)), \forall (l_{i,j}^p) \in L_p. \tag{15}$$

Here, $\Omega(n_p^k)$ denotes the neighbors of n_p^k. Constraint (10) ensures that every virtual node is mapped to one and only one physical node. Conversely, constraint (11)limits each physical node to hosting at most one virtual node, thus enforcing a unique mapping relationship due to isolation requirements. Constraint (12) verifies that virtual nodes are allocated to physical nodes with adequate resources. Following the principle of flow conservation, constraint 13 guarantees that each virtual link (n_v^m, n_v^w) is routed along a physical path from n_p^i (the physical node where n_v^m is placed) to n_p^j (the physical node where n_v^w is placed). Constraint (14) eliminates the possibility of routing loops, thereby ensuring that virtual links are routed acyclically. Lastly, constraint 15 ensures that the bandwidth usage on each physical link remains within its available capacity. Overall, constraints (10,11,12) enforce the one-to-one placement and computing resource availability required in the node mapping process. And constraints (13,14,15) ensure the path connectivity and bandwidth resource availability asked in the link mapping process.

C. Preliminary Study

We have conducted a preliminary study to highlight the motivation to handle failure samples and unsolvable instances. In this study, we trained a representative baseline model, A3C-GCN (Zhang et al., 2024b), which shares a solution construction paradigm similar to our approach and uses a penalty mechanism to handle all failure samples. The training was conducted with various arrival rates for VN requests because it is evident that increasing the arrival rate of VN requests leads to a higher frequency of unsolvable instances. After training, we tested the models using a fixed arrival rate $\lambda = 0.14$ (the same as in Section 4.1: Experimental Settings) with a seed of 0 as the benchmark.

λ for Training	VN_RAC ↑	LT_R2C ↑	LT_REV ($\times 10^7$) ↑
0.14	0.734	0.537	8.707
0.18	0.721	0.455	8.699
0.22	0.679	0.488	7.578
0.26	0.666	0.482	7.397

Table 2: The testing performance of baseline A3C-GCN trained under various λ values.

The results are shown in Figure 2. We observe that as the arrival rate of VN requests increases, the A3C-GCN model trained under higher arrival rates exhibits worse performance. Due to the increased proportion of unsolvable instances, the caused failure samples interfere more strongly with the center of policy optimization, making it difficult to learn a high-quality solution strategy. This indicates that this method struggles to effectively handle unsolvable instances during training, which negatively impacts the optimization robustness and overall performance.

D. Model Details

In this section, we present the key concepts, theoretical foundations, explanation of CONAL's components, and descriptions of both the training and inference processes for CONAL.

D.1. Illustrative Explanation of Prepared Incident Links

To make reader clearly understand the prepared incident links, we provide a brief illustrative example of this concept in Figure 3. Considering the third decision timestep, after mapping virtual nodes n_v^1 and n_v^2 onto physical nodes n_p^1 and n_p^2, we aim to find a physical node to host the to-be-placed virtual node n_v^3. When attempting to place n_v^3 onto n_p^3, we need to consider the routing of virtual links (n_v^1, n_v^3) and (n_v^2, n_v^3) whose endpoints are now both placed. In this example, (n_v^1, n_v^3) and (n_v^2, n_v^3) are called prepared incident links. For current decision timestep, we need to route all of them with connective physical paths while ensuring resource constraints are met.

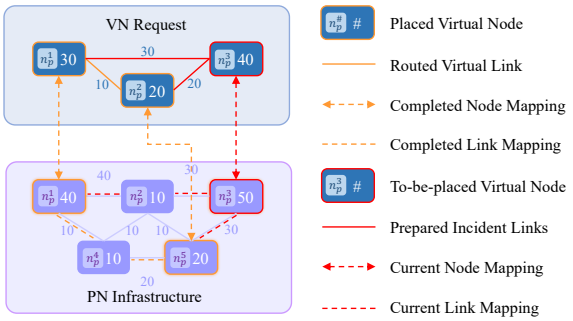

Figure 3: An illustrative example of prepared incident links.

D.2. Proof of Lagrange Multiplier Convergence

Proposition D.1. *During online training, if there exists an instance without any feasible solution (i.e. $H(s) > 0, \forall s \in S$), then the Lagrange multiplier can become infinite.*

Proof. According to the optimality condition of Karush-Kuhn-Tucker (KKT), any optimal solution to the constrained optimization problem (4) must satisfy three conditions: the feasibility condition, the non-negativity condition, and the complementary slack condition, expressed as follows:

$$\begin{aligned} H(s) &\leq 0, \\ \lambda &\geq 0, \\ \lambda \cdot H(s) &= 0. \end{aligned} \tag{16}$$

Given that $H(s) > 0, \forall s \in S$, the primal feasibility condition is violated; there are no feasible solutions that satisfy $H(s) \leq 0$. The complementary slackness condition requires that for each $s \in S$, either $\lambda = 0$ or $H(s) = 0$. Since $H(s) > 0$, we must have $\lambda = 0$ to satisfy this condition. However, setting $\lambda = 0$ does not penalize the constraint violation, and the primal feasibility condition remains unsatisfied. This leads to a contradiction: there is no finite $\lambda \geq 0$ that satisfies all the KKT conditions when $H(s) > 0, \forall s \in S$. The optimization problem is infeasible because the constraints cannot be met. In practical online training, the Lagrange multiplier λ is adjusted iteratively to enforce the constraints by increasing λ whenever the constraints are violated. Since $H(s) > 0$ always holds, the Lagrange multiplier λ will continually increase in an attempt to penalize constraint violations. As a result, λ can become arbitrarily large, theoretically approaching infinity.

□

D.3. Heterogeneous Graph Network

To encode the topological and attribute information of G_I, we enhance widely-used graph attention networks (GAT) (Veličković et al., 2018) by integrating heterogeneous link fusion and link attribute encoding in the propagation process. We begin by using the MLPs to generate the representations of virtual and physical nodes, i.e., $H_v^0 = \mathrm{MLP}(X_v^n), H_p^0 = \mathrm{MLP}(X_p^n)$. Then, we leverage K layers of GNNs to assimilate the topological and bandwidth information. At each κ-th layer, a link feature-aware GAT extracts all node latent representations independently across different link types:

$$\bar{H}_v^\kappa = \mathrm{GAT}(H_v^{\kappa-1}, L_v, X_v^l), \quad \bar{H}_p = \mathrm{GAT}(H_p^{\kappa-1}, L_p, X_p^l), \tag{17}$$

$$Z_{v,m}^\kappa, Z_{p,m}^\kappa = \mathrm{GAT}\left(\left[Z_v^{\kappa-1}; Z_p^{\kappa-1}\right], L_{v,p,m}, X_{v,p,m}^l\right), \tag{18}$$

$$Z_{v,d}^\kappa, Z_{p,d}^\kappa = \mathrm{GAT}\left(\left[Z_v^{\kappa-1}; Z_p^{\kappa-1}\right], L_{v,p,d}, X_{v,p,d}^l\right). \tag{19}$$

Here, ; denotes the combination operator. Particularly, when calculating the attention weight between node i and j using their representation h_i and h_j, we also apply the MLP to their link attribute $x_{i,j}^l$, i.e., $h_{i,j} = \mathrm{MLP}(x_{i,j}^l)$, and incorporate it into this process to perceive bandwidth resources:

$$a_{i,j} = \frac{\exp(\mathrm{MLP}(z_i + z_j + z_{i,j}))}{\sum_{k \in \mathcal{N}(i)} \exp(\mathrm{MLP}(z_i + z_k + z_{i,k}))}, \tag{20}$$

where $\mathcal{N}(i)$ indicates the neighbor set of node i.

Then, to aggregate the diverse information presented through different link perspectives, we apply the sum pooling method to produce the node representations for each GNN layer:

$$Z_v^\kappa = \bar{Z}_v^\kappa + Z_{v,m}^\kappa + Z_p^\kappa, \quad Z_p^\kappa = \bar{Z}_p^\kappa + Z_{p,m}^\kappa + Z_{p,d}^\kappa. \tag{21}$$

Finally, leveraging the final layer representations, H_v^K and H_p^K, alongside residual connections to bolster initial feature representation, we obtain the final representations of all nodes $Z = \{Z_v, Z_p\}$:

$$Z_v = Z_v^K + Z_v^0, \quad Z_p = Z_p^K + Z_p^0. \tag{22}$$

D.4. Barlow Twins Loss Function

In this work, we utilize the contrastive learning method to bring the representations under augmented views close to enhance the awareness of bandwidth-constrained path connectivity. One of the main directions of contrastive learning is to utilize both positive and negative sample distinctions (Oord et al., 2018; Chen et al., 2020). However, in our application, generating and selecting negative samples that are markedly different in terms of feasibility semantics is significantly challenging. This difficulty can adversely affect the learning quality and the generalizability of the models. Therefore, considering multiple views of the graph with the same feasibility semantics, we focus on eschewing negative samples altogether while preventing feature collapse, an emerging direction of contrastive learning (Grill et al., 2020; Zbontar et al., 2021). Specifically, we adopt the Barlow Twins method (Zbontar et al., 2021) for its simplicity and effectiveness, which circumvents negative sample selection and maintains the original network architecture. Given the node embeddings under two augmented views, H^a and H^b, we reduce redundancy between embedding components by aligning their cross-correlation matrix with the identity matrix/ Specifically, we engage the subsequent optimization with following unsupervised learning loss objective function:

$$L_{CL} = \sum_i (1 - \mathbb{C}_{ii})^2 + w \sum_i \sum_{i \neq j} \mathbb{C}_{ij}^2, \tag{23}$$

where the first one is the invariance term and the second one is the redundancy reduction term. w is tradeoff weight. $\mathbb{C}_{ij}$ is the cross-correlation matrix computed between the output node representations of the two identical networks along the batch dimension: $\mathbb{C}_{ij} = \frac{\sum_b Z^A_{b,i} Z^B_{b,j}}{\sqrt{\sum_b \left(Z^A_{b,i}\right)^2} \sqrt{\sum_b \left(Z^B_{b,j}\right)^2}}$. Here, b indexes node samples. i, j index the node representation dimension, respectively. Subsequently, we will equip our final optimization objective with this unsupervised learning loss function.

D.5. Lagrangian-based PPO Training Method.

To optimize the policy for VNE solving, we adopt the Lagrangian-based actor-critic framework with PPO (Ray et al., 2019) objective as our training algorithm, which incorporates constraint guarantees within the RL training process (Schulman et al., 2017). In practical implementation, we derive the node representations Z_v and Z_p from the state s, with our constraint-aware graph representation method. These representations serve as inputs to a policy network, which generates an action distribution, $\pi(s) = \mathrm{MLP}(Z^p) \in \mathbb{R}^{|N_p|}$, used for the action selection. Additionally, we employ three additional networks: the value critic network V_r^π, the reachability critic network V_h^π, and the Lambda network Λ^π. They have similar architectures, $\forall V \in \{V_r^\pi, V_h^\pi, \Lambda^\pi\}, V(s) = \mathrm{MLP}\left(\sum_{z \in Z_p} z\right) \in \mathbb{R}^1$. They estimate cumulative rewards, constraint violations, and the Lagrangian multiplier λ, respectively. We optimize V_r^π and V_h^π with mean squared error (MSE) losses, denoted as L_r and L_h, comparing predicted values against actual results for cumulative rewards and violations, respectively. The Lambda network (Ma et al., 2021) is updated to optimize the balance between performance and safety, according to:

$$L_{LAM} = \Lambda^\pi(s) \cdot (V_h^\pi(s) - D_h^{\pi'}(s)). \tag{24}$$

The objective function for the policy network within the PPO framework is expressed as:

$$L_{PPO}(\pi) = \mathbb{E}[\min(r(\pi)A_t, \mathrm{CLIP}(r(\pi), 1-\epsilon, 1+\epsilon)A_t)], \tag{25}$$

where A_t represents the advantage function at time step t, and $r(\pi) = \frac{\pi(s_t, a_t)}{\pi^{old}(s_t, a_t)}$ calculates the ratio of the probabilities for the selected action between the current and previous policies. The CLIP function limits policy updates to enhance stability.

Finally, integrating the unsupervised contrastive learning objective L_{CL} in the path-bandwidth contrast method, our comprehensive loss function in the training process is formulated as follows:

$$L = w_{PPO} \cdot L_{PPO} + w_r \cdot L_r + w_h \cdot L_h + w_{LAM} \cdot L_{LAM} + w_{CL} \cdot L_{CL}, \tag{26}$$

where all $w_{(\cdot)}$ denote the weights of loss objectives.

D.6. Detailed Analysis of Computational Complexity

CONAL exhibits a computational complexity of $O\left(|N_v| \cdot K \cdot \left(|L_p|d + |N_p + N_v|d^2\right)\right)$, which the complexities other baseline methods based on RL and GNNs are $O\left(|N_v| \cdot K \cdot \left(|L_p|d + |N_p|d^2\right)\right)$. Here, N_v and L_v denote the number of virtual nodes and links, N_p and L_p denote the number of physical nodes and links, K denotes the number of GNN layers, and d denotes the embedding dimension. Concretely, When constructing a solution for one VNE instance, CONAL performs inference N_v times with the GNN policy, similar to most RL and GNN-based methods. The difference in complexity between CONAL and RL/GNN-based baselines mainly arises from the different neural network structures used, such as GAT and GCN. One GAT and one GCN layer have the same complexity, both $O\left(|L|d + |N|d^2\right)$, where $|N|$ and $|L|$ denote the number of nodes and links [a]. In CONAL, we enhance the GAT with the heterogeneous modeling for the interactions of cross-graph status. Each heterogeneous GAT layer consists of three types of GAT layers for VN, PN, and cross-graph interactions (the number of links between virtual and physical nodes is always N_p). The complexities for these layers are $O\left(|L_v|d + |N_v|d^2\right)$, $O\left(|L_p|d + |N_p|d^2\right)$, and $O\left(|N_p|d + |N_p + N_v|d^2\right)$, respectively. Each heterogeneous GAT layer consists of three types of GAT layers for VN, PN, and cross graph (the number of links between virtual and physical node always is N^p), whose complexity is $O\left(|L_v|d + |N_v|d^2\right)$, $O\left(|L_p|d + |N_p|d^2\right)$, and $O\left(|N_p|d + |N_p + N_v|d^2\right)$. Considering that $|N_v|$ is significantly smaller than $|L_v|$ and typically $L_p > N_p$ in practical network systems, the overall complexity of CONAL is $O\left(|N_v| \cdot K \cdot \left(|L_p|d + |N_p + N_v|d^2\right)\right)$. In comparison, other RL and GNN-based methods separately encode VN and PN with GAT or GCNs, without considering GNN layers for cross-graph interactions, leading to their complexities being $O\left(|N_v| \cdot K \cdot \left(|L_p|d + |N_p|d^2\right)\right)$. Overall, while CONAL slightly increases the complexity compared to existing RL and GNN-based methods due to its heterogeneous modeling approach, it achieves significant performance improvements.

E. Descriptions of Training and Inference Process

In this section, we summarize the training and inference process of CONAL in Algorithm 1 and Algorithm 2, respectively.

E.1. Training Process of CONAL

Algorithm 1 Training process of CONAL.

Input: A set of VNE instances $\mathcal{I}$
Output: A learned policy π
Initialize the policy network π, value critic network V_r^π, feasibility critic network V_h^π, and lambda network Λ^π with random weights
Initialize the surrogate policy network π' same as the policy network π
 # Stage 1: Experience Collection
for each VNE instance $I \in \mathcal{I}$ **do**
  Compute adaptive reachability budget $D_h^{\pi'}(s)$ for the following sampled state s using π'
  Initialize state s_0 from the heterogeneous graph G_I and its augmented views G_I^A and G_I^B
  for timestep $t = 0$ to T **do**
    Generate the action probability distribute and select action $a_t \sim \pi(\cdot|s_t)$
    Execute action a_t, observe reward r_t and next state s_{t+1}
    Compute constraint violation $h_t = H(s_{t+1})$ and cost $c_t = C(s_{t+1})$
    Store transition $(s_t, a_t, r_t, s_{t+1}, h_t, c_t, D_h^{\pi'}(s_t))$ in trajectory memory τ
  end for
end for
 # Stage 2: Policy Optimization
for each update step **do**
  Sample a batch of transitions from the trajectory memory τ
  Calculate the PPO objective L_{PPO} for policy π with Eq. 25
  Calculate the value critic loss L_r and reachability critic loss L_h
  Calculate the loss of Lambda network with Eq. 24
  Calculate the contrastive loss L_{CL} with the Barlow Twins method, i.e., Eq. 23
  Obtain the final loss with Eq. 25 and update π, V_r^π, V_h^π, and Λ^π
  if update the surrogate policy **then**
    Synchronize the parameters of π' with π, i.e., $\pi' \leftarrow \pi$
  end if
end for
return: The learned policy π

The training process of CONAL begins by randomly initializing the neural networks: the policy network π, value critic network V_r^π, feasibility critic network V_h^π, and lambda network Λ^π. The training involves two key stages: experience collection and policy optimization. Through these stages, we iteratively update the neural networks and ultimately learn the policy. This training process is outlined in Algorithm 1.

During the experience collection stage, for each incoming instance $I \in \mathcal{I}$, we utilize the surrogate policy π' to preemptively solve this instance I. The maximum constraint violation caused by π' is regarded as adaptive reachability budgets $D_h^{\pi'}(s)$ for the following states s sampled by main policy π. At each decision timestep t, we build a heterogeneous graph G_I based on the current situation of instance I. We also construct two augmented views, G_I^A and G_I^B, with the proposed feasibility-consistency augmentations, which will be used in the calculation of contrastive loss. The state s_t is then extracted from G_I, G_I^A and G_I^B. Based on the state s_t, the policy π extracts information with the heterogeneous graph network and selects an action a_t. Then, the environment executes this action, transits into the next state s_t, and returns the reward r_t, violations h_t and costs c_t. These items collectively form a transition $(s_t, a_t, r_t, s_{t+1}, h_t, c_t, D_h^{\pi'}(s_t)$ and stored in a trajectory memory τ.

In the subsequent policy optimization stage, we iteratively sample batches of transitions from the trajectory memory τ to update neural networks. Then, we calculate various losses, including the PPO loss L_{PPO}, value critic loss L_r, reachability critic loss L_h, and Lambda network loss L_{LAM}. Additionally, we integrate our proposed unsupervised contrastive loss L_{CL}

in path-bandwidth contrast during training. Overall, we calculate the weighted sum of these losses as the final loss L and update neural networks. If necessary, we synchronize surrogate policy π' with the main policy π.

E.2. Inference Process of CONAL

Algorithm 2 Inference process of CONAL.

Input: An arrived VNE instance I; The learned policy π
Output: The solution status
Initialize state s_0 from the heterogeneous graph G_I
for timestep $t = 0$ to T **do**
  Generate the action probability distribute and select action $a_t \sim \pi(\cdot|s_t)$
  Execute action a_t: Map the to-be-decided virtual node n_v^t onto the selected physical node a_t
  Transit to next state s_{t+1}: Route all prepared incident links n_v^t
  Compute constraint violation $h_t = H(s_{t+1})$ and cost $c_t = C(s_{t+1})$
  if any constraints are violated, i.e., $c_t > 0$ **then**
    return FALSE
  end if
end for
return TRUE

Note that the surrogate policy and the path-bandwidth contrast module are not utilized in this process. During the inference process, we use the learned policy π to solve newly arrived VNE instances, which is outlined in Algorithm 2.

At each decision timestep t in the inference process, we attempt to place the virtual node n_v^t, and route its prepared incident links $\delta'(n_v^t)$, until the solution is successfully completed or any constraints are violated. Concretely, we extract the state features s_t from the heterogeneous graph, and input them into the policy network to produce an action probability distribution $\pi(a_t \mid s_t)$. The action a_t, representing the selected physical node, is chosen using a greedy strategy that picks the action with the highest probability. Then, we execute the selected action, i.e., mapping the virtual node n_v^t onto the physical node a_t. Once the action is executed, the network system transitions to the next state s_{t+1}, where all prepared incident links $\delta'(n_v^t)$ are routed. Subsequently, the system computes the corresponding constraint violations h_t and costs c_t for the current state. If any constraints are violated during the process, the inference is terminated early, and the instance is rejected. Otherwise, the process continues until a complete and feasible solution is found.

F. Experimental Details

In this section, we provide the details of implementations and hyperparameter settings, the descriptions of compared baselines and CONAL's variations, and the definition of metrics.

F.1. Implementation Details

CONAL Implementation. We implement the GNNs in CONAL with PyG and other neural networks of CONAL with PyTorch. Each neural network has a hidden dimension of 128 and GAT modules are composed of 3 layers. We set the both reward and cost discounted factor λ of CMDP to 0.99. We set the augment ratio ϵ in the path-bandwidth contrast method to 1. We use a batch size of 128 and the Adam optimizer (Kingma & Ba, 2014) with a learning rate of 0.001. We use the sampling strategy and greedy strategy for the action section in the training and testing processes, respectively. For the k-shortest path algorithm used in link routing, we set the maximum path length k to 5. The loss weights are set as follows: $w_{PPO} = 1.0$, $w_{LAM} = 0.1$, $w_{CL} = 0.001$, $w_r = 0.5$ and $w_h = 0.5$.

Simulation for Training and Testing. For RL-based methods and CONAL, we train policies for each average arrival rate η, where running seeds are randomly set in every simulation. During testing, we evaluate the performance of all algorithms by repeating the tests with 10 different seeds (i.e., $0, 1111, 2222, \cdots, 9999$) for each η to ensure statistical significance.

Computer Resources. All experiments were conducted on a Linux server equipped with one NVIDIA A100 Tensor Core GPU, 24 AMD EPYC 7V13 CPUs, and 128GB of memory.

F.2. Baseline Descriptions

We introduce the compared baselines, which cover the most perspectives of VNE solving strategies:

- **NRM-VNE** (Zhang et al., 2018) is a node ranking-based heuristic method. It first uses a Node Resource Management (NRM) metric to rank both virtual and physical nodes and employs a greedy matching approach for node mapping. Then, for link mapping, this method utilizes the k-shortest path algorithm, similar to our approach.
- **GRC-VNE** (Gong et al., 2014) is a node ranking-based heuristic method. It sorts nodes with a Global Resource Control (GRC) strategy based on random walk and maps them accordingly. Then, it conducts the link mapping using k-shortest path algorithm.
- **NEA-VNE** (Fan et al., 2023) is a node ranking-based heuristic that employs a Node Essentiality Assessment (NEA) metric to rank nodes and follows a similar mapping as NRM-VNE and GRC-VNE.
- **GA-VNE** (Zhang et al., 2019) is a meta-heuristic method based on genetic algorithms. It models each node mapping solution as a chromosome and iteratively explores the solution space by simulating the process of natural selection and genetic evolution.
- **PSO-VNE** (Jiang & Zhang, 2021) is a meta-heuristic method that employs particle swarm optimization. It explores the VNE solution space by simulating the behavior of particles.
- **MCTS-VNE** (Haeri & Trajković, 2017) is a model-based RL method. It utilizes the Monte Carlo Tree Search (MCTS) algorithm to explore possible solutions with upper confidence bound strategies.
- **PG-CNN** (Zhang et al., 2022) is a model-free RL method. It models the solution construction of each VNE instance as MDP. Then, it develops a policy network with Convolutional Neural Network (CNN) and trains it using the Policy Gradient (PG) algorithm. To avoid unnecessary failure during action selection, a mask vector is applied to ensure that only physical nodes with sufficient computing resources are selected. Specifically, during training, only samples related to feasible solutions are used for optimization.
- **DDPG-ATT** (He et al., 2023a) is a model-free RL method that builds an ATTention-based (ATT) policy network and uses the Deep Deterministic Policy Gradient (DDPG) algorithm for training.
- **A3C-GCN** (Zhang et al., 2024b) is a model-free RL method. It constructs a policy network with a Graph Convolutional Network (GCN) and a Multi-Layer Perceptron (MLP). The Asynchronous Advantage Actor-Critic (A3C) algorithm is used for training. It also adopts the masking mechanism in action probability distribution for only selecting physical nodes with enough computing resources/ Particularly, during training, if encountering failure samples, customized negative rewards are returned. It also uses the probability distribution action masking mechanism. Similar to A3C-GCN, it introduces the penalty into reward shaping.
- **GAL-VNE** (Geng et al., 2023) is a model-free RL method that formulates VNE into both Global learning across requests And Local prediction within requests (GAL). It first uses supervised learning to develop a GNN policy to solve VNE in one shot. Then, in online perspective, they use RL to finetune this policy to improve overall performance.

Regarding the baseline implementation, we use the official code of GAL-VNE and reproduce DDPG-ATT following the original paper. For the other baselines, we derive their implementations from the Virne[1] library. Furthermore, for their hyperparameter settings, we follow the original papers for heuristic baselines. For RL-based baselines, we set the same hidden size of their neural networks as us and other hyperparameters according to their original papers. In the link mapping process, all baselines use the same k-shortest path algorithm as ours.

F.3. Variations Descriptions

To verify the individual performance contributions of each CONAL's components, we design the following variations as additional baselines:

[1] https://github.com/GeminiLight/virne

- **CONAL$_{\text{w/o HM}}$** discards the proposed heterogeneous modeling (HM) module. Instead, it independently extracts the features of VN and PN using GAT. The global representation of VN is obtained using the sum pooling method. Then, we produce the final node representation of PN by adding this global representation, which is enhanced with the path-bandwidth contrast module and used to produce the final action probability distribution.
- **CONAL$_{\text{w/o PC}}$** removes the proposed path-bandwidth contrast (PC) module.
- **CONAL$_{\text{w/o HM \& PC}}$** omits both the HM and PC modules, utilizing independent feature extractions of VN and PN and an addition-based fusion method, same as CONAL$_{\text{w/o HM}}$.
- **CONAL$_{\text{w/o REACH}}$** replaces our reachability-guided optimization objective (i.e., Eq. 3) with the traditional cumulative cost optimization objective (i.e., Eq. 2), which restricts expected cumulative costs below zero. It extend the proposed adaptive reachability budget, i.e., Eq. 5, to calculate adaptive cost budget, defined as follows:

$$\forall s \in \tau, D_c^{\pi'}(s) = \sum_{s' \in \tau'} C(s'). \tag{27}$$

- **CONAL$_{\text{w/o ARB}}$** removes the proposed adaptive reachability budget (ARB) and uses zero as a fixed reachability budget.

F.4. Metric Definitions

We provide detailed definitions of key evaluation metrics that are widely used to evaluate the effectiveness of VNE algorithms comprehensively (Fischer et al., 2013; Yan et al., 2020):

- VN Acceptance Rate (**VN_ACR**) measures the proportion of VN requests that are successfully accepted by the system. It evaluates the ability of network provider to satisfy user service requests, defined as

$$\text{VN_ACR} = \frac{\sum_{t=0}^{\mathcal{T}} |\tilde{\mathcal{I}}(t)|}{\sum_{0}^{\mathcal{T}} |\mathcal{I}(t)|}, \tag{28}$$

  where $\mathcal{I}(t)$ and $\tilde{\mathcal{I}}(t)$ denote the set of totally arrived and accepted VNE instances at the unit of time slot t. The operation $|\mathcal{I}|$ means the number of VN requests in the set $\mathcal{I}$.

- Long-term Revenue (**LT_REV**) evaluates the total revenue generated over a specified period, serving as an indicator of the financial gains derived from the VN requests processed by the system. It reflects the economic impact of decisions on network operations.

$$\text{LT_REV} = \sum_{t=0}^{\mathcal{T}} \sum_{I \in \tilde{\mathcal{I}}(t)} \text{REV}(E) \times \varpi, \text{ where } E = f_G(I). \tag{29}$$

  Here, ϖ the lifetime of the tackled VN G_v, where $I = \{G_v, G_p\}$.

- Long-term Revenue-to-Consumption Ratio (**LT_R2C**) quantifies the economic efficiency of the system by comparing the revenue generated to the resources consumed. It offers insights into the operational cost-effectiveness of the VNE solutions implemented.

$$\text{LT_R2C} = \frac{\sum_{t=0}^{\mathcal{T}} \sum_{I \in \tilde{\mathcal{I}}(t)} \text{REV}(E) \times \varpi}{\sum_{t=0}^{\mathcal{T}} \sum_{I \in \tilde{\mathcal{I}}(t)} \text{CONS}(E) \times \varpi}, \text{ where } E = f_G(I). \tag{30}$$

- Average Solving Time (**AVG_ST**) measures the computational efficiency of VNE algorithm in online inference. We define it as the average wall-clock time required to solve a single instance during one simulation, and use second (s) as the time unit.
- Constraint Violation (**C_VIO**) assesses the constraint satisfaction ability of the VNE algorithm, which is used to compare the constraint awareness of CONAL and its variations. It is defined as cumulative constraint violations over all VNE instances in one simulation:

$$\text{C_VIO} = \sum_{t=0}^{\mathcal{T}} \sum_{I \in (\mathcal{I}(t) - \tilde{\mathcal{I}}(t))} \sum_{s \sim \tau} C(s), \tag{31}$$

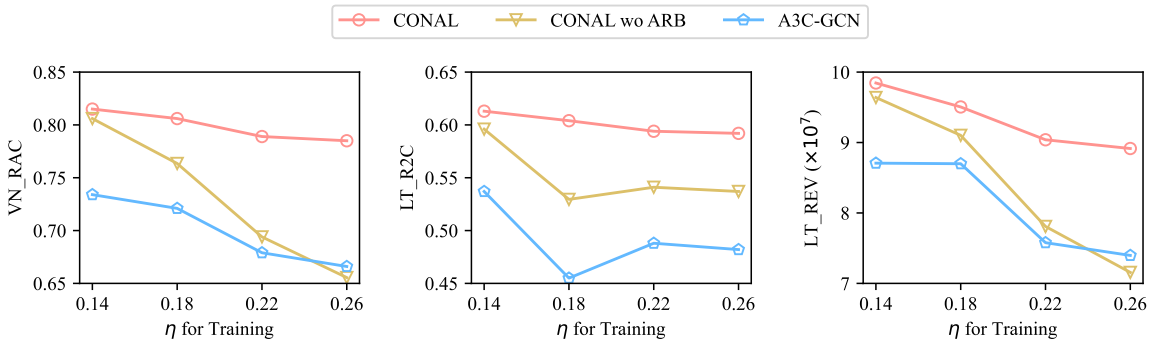

(a) VN_RAC vs. η (b) LT_R2C vs. η (c) LT_REV vs. η

Figure 4: Results on testing performance (η = 0.14) of algorithms trained under different average arrival rate η.

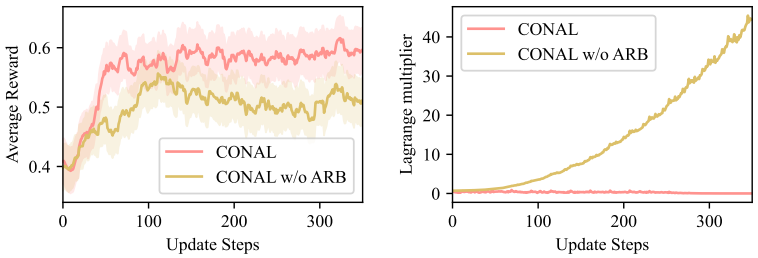

(a) Learning curves (b) Lagrange multiplier convergence

Figure 5: Training convergence curves of reward and Lagrange multiplier (η = 0.26 for training).

where τ is the trajectory produced by the policy π with greedy selection and $C(s)$ is the caused violations in state s. $\sum_{s\sim\tau} C(s)$ means the sum of violations in the trajectory τ.

G. Addtional Evaluation

In this section, we present additional experiments to evaluate the training stability, generalizability, scalability, and practicability of CONAL, as well as investigate the impact of two key hyperparameters.

G.1. Training Stability Study

To study the training stability of CONAL, we first provide an analysis of how different training conditions impact testing performance. Then, we dive into the convergence comparison between CONAL and CONAL$_{\text{w/o ARB}}$.

Training Conditions vs. Testing Performance Analysis. Similar to our preliminary study in Appendix C, we further explore the impact of training conditions on CONAL performance. We train CONAL, CONAL$_{\text{w/o ARB}}$ and A3C-GCN under different arrival rates λ of VN requests from 0.14 to 0.26, as higher arrival rates increase the frequency of unsolvable instances. After training, we evaluate the models using a fixed arrival rate of $\lambda = 0.14$ with a random seed of 0 as the benchmark. The results are shown in Figures 4(b)(c)(d). We observe that as the arrival rate λ of training conditions increases, CONAL maintains a more stable testing performance while CONAL$_{\text{w/o ARB}}$ and A3C-GCN shows an noticeable decline. Specifically, when trained under $\lambda = 0.26$, which includes more unsolvable instances, two metrics (VN_RAC and LT_REV) of CONALw/o ARB even perform worse than A3C-GCN, which incorporates a penalty in the reward function. This may be because, while CONAL$_{\text{w/o ARB}}$ can perceive fine-grained constraints and aims to achieve zero violation, without the ARB module and the penalty in the reward function, it struggles to handle the increased number of *failure samples* caused by *unsolvable instances* effectively. This analysis shows that CONAL with the proposed ARB module is more stable in learning a high-quality policy by efficiently handling unsolvable instances and perceiving complex constraints.

Training Convergence Analysis. To investigate the training convergence of CONAL and CONAL$_{\text{w/o ARB}}$, particularly training with a high proportion of unsolvable instances, we conduct experiments with an arrival rate $\eta = 0.26$ for VN requests on WX100, which corresponds to a scenario with more unsolvable instances. During training, we monitor both reward and Lagrange Multiplier over 300 training steps. (a) *Learning Curve Comparison*. We first compare the learning

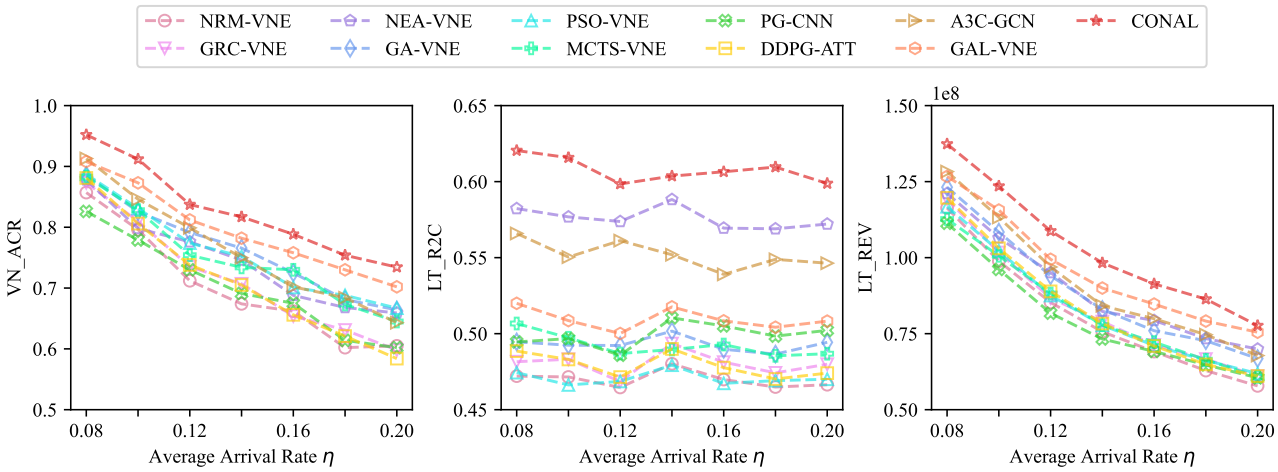

(a) VN Acceptance Rate (b) Long-term R2C Ratio (c) Long-term Revenue

Figure 6: Results in the sensitivity study on varying average arrival rate η.

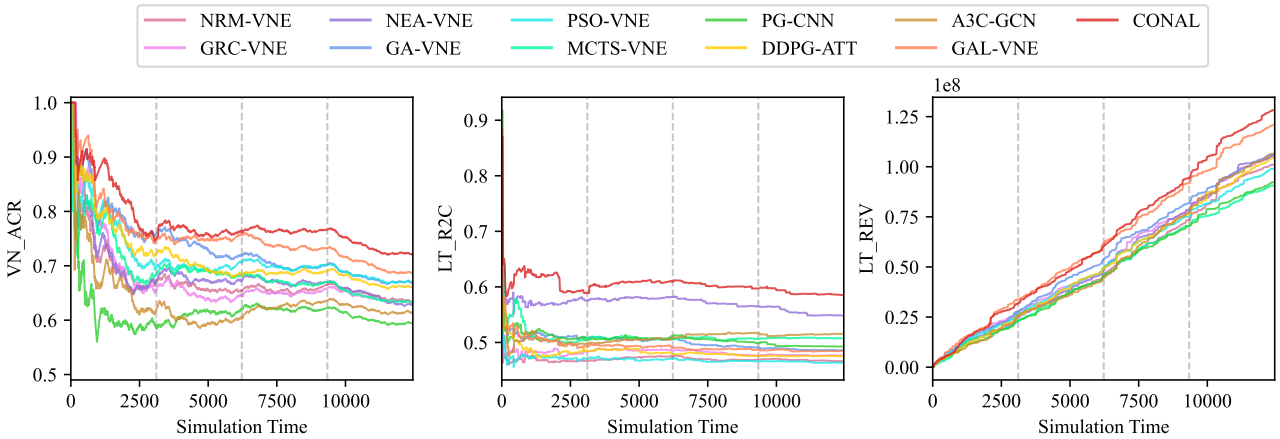

(a) VN Acceptance Rate (b) Long-Term R2C Ratio (c) Long-Term Revenue

Figure 7: Results in the dynamic request distribution testing. The gray vertical lines roughly partition the request processing stages into four groups with different distributions.

curves of CONAL and $\text{CONAL}_{\text{w/o ARB}}$, depicted in Figure 5(a). We observe that compared to $\text{CONAL}_{\text{w/o ARB}}$ fluctuates during the training process, CONAL exhibits greater stability and converges to better performance This stability and superior performance are attributed to our adaptive reachability budget method, which effectively addresses unsolvable instances during training, thus enhancing overall training stability and mitigating negative impact on performance. (b) *Convergence Analysis of Lagrange Multiplier*. As shown in Figure 5(b), the results reveal a clear distinction in the convergence behavior of λ. Without ARB, λ diverges rapidly to extreme values. This divergence reflects instability in the optimization process and leads to unreliable policy updates. In contrast, CONAL with ARB effectively stabilizes λ throughout training, close to a small value. By dynamically adjusting the feasibility budget, ARB mitigates the impact of unsolvable instances, ensuring stable training even under challenging conditions. These findings demonstrate the crucial role of ARB module in preventing numerical instability and enabling robust policy learning in scenarios with high unsolvability.

G.2. Generalizability Study

To evaluate the robustness and adaptability of CONAL's trained policy across various network conditions, we conduct a series of experiments to test its generalizability in different dynamic and fluctuating environments, i.e., under varying request frequencies and changing resource demands.

Request Frequency Sensitivity Study. We analyze the sensitivity of CONAL and other VNE algorithms to varying arrival

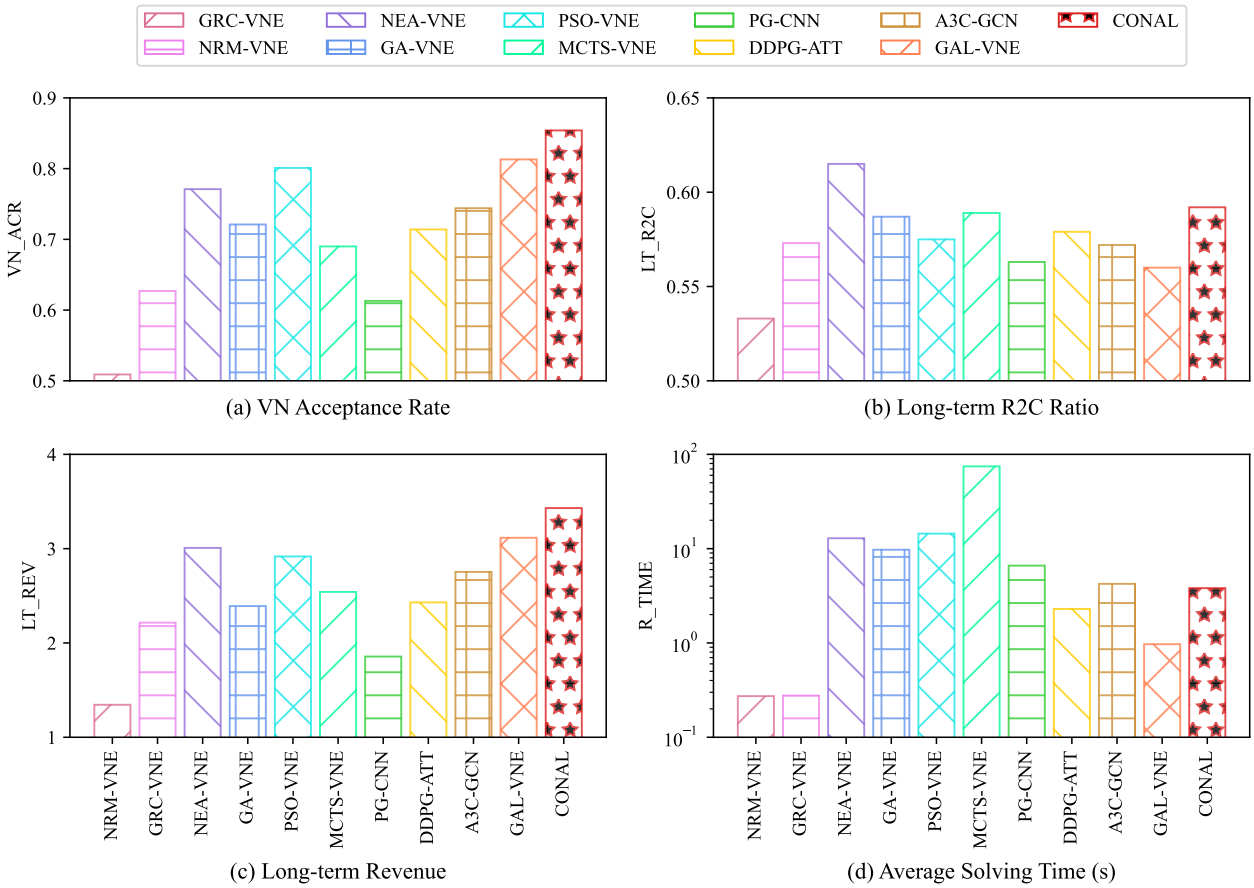

(a) VN Acceptance Rate (b) Long-term R2C Ratio

(c) Long-term Revenue (d) Average Solving Time (s)

Figure 8: Results in scalability validation.

rates of VN requests by adjusting the value of η. This manipulation simulates different network system scenarios with varying traffic throughputs. Specifically, we conduct experiments with η values ranging from 0.08 to 0.20, in increments of 0.02. The results are illustrated in Figure 6. As request frequency η increases, we observe all algorithms exhibit a clear downward trend in VN_ACR. This is mainly because the increase in request frequency intensifies resource competition among VN requests at the same moment, resulting in more rejections of VNs. In particular, CONAL consistently outperforms the compared baseline algorithms across all tested values of η. This indicates that CONAL is more effective and adaptable to changes in request frequency, maintaining superior performance. Overall, this analysis highlights the effectiveness of CONAL in handling complex network environments with fluctuating traffic throughput.

Dynamic Request Distribution Testing. In practical scenarios, the node size and resource requirements distributions of VN requests may vary due to different service demands. To simulate such situations, similar to previous work (Geng et al., 2023), we equally divided 1000 VN requests into four sub-groups. In comparison to the default simulation settings, we modified one parameter related to the distribution of VN resource demand or VN node size for each sub-group: For the first group, the node and link resource distributions of VN are changed to [0, 30] and [0, 75], respectively; For the second group, the node and link resource distributions of VN are adjusted to [0, 40] and [0, 100], respectively; For the third group, the VN node size distribution is changed to [2, 15]; For the fourth group, the VN node size distribution is altered to [2, 20]. We evaluate the CONAL and other RL-based methods trained in the default settings. The results are illustrated in Figure 7. We observe that CONAL exhibits superior performance across all metrics, indicating its strong adaptability to dynamic request distributions. Regarding the VN_ACR, all algorithms experience a rapid decrease in the early stages of the simulation due to the quick consumption of resources. Subsequently, their VN_ACR becomes relatively stable. It is worth noting that in the fourth stage, most algorithms show a clear downward trend in VN_ACR. This is because embedding larger VNs with more complex topologies and greater resource demands becomes increasingly challenging. This testing shows that CONAL is highly adaptable across varying VN request distributions, which underscores CONAL's generalization in dynamic systems.

G.3. Scalability Analysis

In this section, we assess the scalability of CONAL by exploring its performance in large-scale network environments and its time consumption to adapt to varying network sizes.

Large-scale Network Validation. Similar to previous work (Wang et al., 2023), we generate a random Waxman topology (Waxman, 1988) with 500 nodes and nearly 13,000 links, named WX500. This mimics the modern large-scale cloud cluster, which is more challenging due to the increased complexity of the topology. Additionally, we increase the VNE size distribution to a uniform range from 2 to 20 nodes, and set the arrival rate of VN requests η to 0.5. All other simulation and hyperparameter settings remain consistent with those outlined in Section 4.1. To adapt the pretrained CONAL model for WX100 to this larger scenario, we fine-tune it on WX500 via transfer learning. The pretraining on WX100 takes approximately 7.274 hours, and the fine-tuning stage on WX500 consumes an additional 4.326 hours. By leveraging transfer learning, we accelerate the training efficiency of CONAL, facilitating the rapid acquisition of a CONAL model suitable for large-scale scenarios. The results are illustrated in Figure 8. We observe that CONAL consistently outperforms the baselines in terms of both VN_ACR and LT_REV. CONAL also demonstrates superior performance in the LT_R2C, which is only marginally lower than NEA-VNE. Regarding the AVG_ST, NEA-VNE, MCTS-VNE, and PSO-VNE exhibit significantly higher time consumption, whereas CONAL maintains a competitive running efficiency similar to PG-CNN, A3C-GCN, and DDPG-ATT. Despite the increased complexity of the WX500 topology, CONAL maintains a balance between performance and computational efficiency. This analysis shows the scalability and efficiency of CONAL in large-scale network scenarios.

Solving Time Scale Analysis. We investigate solving time across different physical network sizes to evaluate CONAL's time scalability. Specifically, we increase the size of physical networks from 200 to 1,000 nodes with a step of 200 to simulate networks of varying scales. Due to enough link connectivity of large-scale network systems, we set the maximum path length k to 4. Figure 9 shows that as the size increases, NRM-VNE, GRC-VNE and GAL-VNE show the most sightly increased average solving time. In contrast, PSO-VNE and GA-VNE experience rapid growth in solving time due to their reliance on extensive search. CONAL exhibits a similar trend with A3C-GCN and DDPG-ATT, since they are all based on constructive solution paradigms. As the size of the physical network increases, the solution time of these algorithms does not explode, still competitive with MCTS and NEA-VNE. Overall, the solving time of CONAL remains efficient even at larger network scales while offering great performance, making it a viable solution for real-time decision-making in large-scale environments.

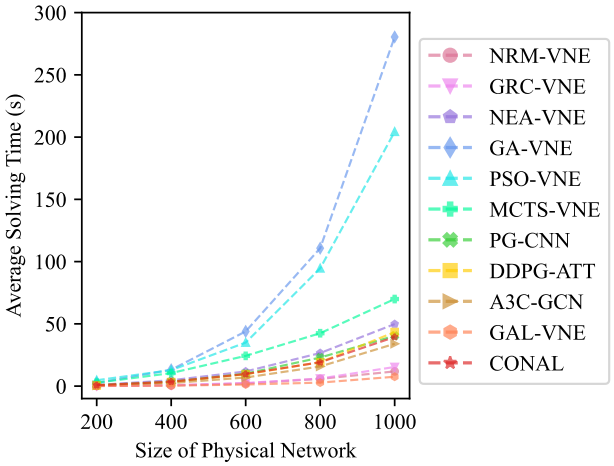

Figure 9: Solving Time Scale with Network Size.

G.4. Real-world Network Topology Validation

To verify the effectiveness of our proposed algorithm in real-world network systems, we conducted experiments on realistic network topologies. Similar to previous works (He et al., 2023a; Wang et al., 2023), we employed two widely-used topologies from SDNlib[2]:

- **GEANT** is the academic research network that interconnects Europe's national research and education networks, comprising 40 nodes, 64 edges, and a density of 0.0821.
- **BRAIN** is the largest real-world network topology in SDNlib, consisting of 161 nodes and 166 edges with a density of 0.0129. It is the high-speed data network for scientific and cultural institutions in Berlin.

Due to the limited resource supply in these topologies, we adjust the average arrival rate η of VN requests to 0.0005 in GEANT and 0.001 in BRAIN. We keep other network system simulation parameters as same as those discussed in Section 4.1. As shown in Table 3, CONAL outperforms all baselines across both network systems in terms of performance metrics. Notably, in the sparser BRAIN topology, RL-based VNE algorithms (e.g., A3C-GCN and GAL-VNE) performed

[2]https://sndlib.put.poznan.pl

Table 3: Results in real-world system validation.

	GEANT			BRAIN		
	VN_ACR ↑	LT_R2C ↑	LT_REV ↑	VN_ACR ↑	LT_R2C ↑	LT_REV ↑
NRM-VNE (Fan et al., 2023)	0.568	0.626	4.169	0.627	0.696	5.189
GRC-VNE (Gong et al., 2014)	0.396	0.574	2.276	0.644	0.652	5.725
NEA-VNE (Fan et al., 2023)	0.739	0.628	7.525	0.656	0.682	5.907
GA-VNE (Zhang et al., 2019)	0.585	0.592	4.362	0.450	0.550	2.512
PSO-VNE (Jiang & Zhang, 2021)	0.525	0.504	3.729	0.415	0.475	2.164
MCTS-VNE (Haeri & Trajković, 2017)	0.573	0.524	4.443	0.494	0.566	2.733
PG-CNN (Zhang et al., 2022)	0.639	0.576	5.712	0.538	0.651	3.804
DDPG-ATT (He et al., 2023a)	0.625	0.533	5.449	0.572	0.657	4.326
A3C-GCN (Zhang et al., 2024b)	0.747	0.692	8.135	0.577	0.715	4.473
GAL-VNE (Geng et al., 2023)	0.804	0.613	9.915	0.591	0.729	4.922
CONAL	**0.916**	**0.761**	**11.946**	**0.683**	**0.835**	**6.339**

* Values in the LT_REV column are scaled by 10^7.

Table 4: Experimental results on the variation of latency-aware VNE.

	VN_RAC ↑	LT_R2C ↑	LT_REV ($\times 10^7$) ↑
NRM-VNE (Fan et al., 2023)	0.655 ± 0.017	0.469 ± 0.005	7.168 ± 0.091
GRC-VNE (Gong et al., 2014)	0.454 ± 0.028	0.509 ± 0.008	5.281 ± 0.281
NEA-VNE (Fan et al., 2023)	0.714 ± 0.014	0.574 ± 0.006	8.186 ± 0.120
GA-VNE (Zhang et al., 2019)	0.717 ± 0.022	0.528 ± 0.004	7.712 ± 0.073
PSO-VNE (Jiang & Zhang, 2021)	0.709 ± 0.020	0.465 ± 0.003	7.457 ± 0.141
MCTS-VNE (Haeri & Trajković, 2017)	0.676 ± 0.017	0.489 ± 0.005	6.882 ± 0.102
PG-CNN (Zhang et al., 2022)	0.659 ± 0.019	0.500 ± 0.004	7.026 ± 0.146
DDPG-ATT (He et al., 2023a)	0.672 ± 0.024	0.477 ± 0.005	7.541 ± 0.096
A3C-GCN (Zhang et al., 2024b)	0.724 ± 0.020	0.552 ± 0.007	8.222 ± 0.125
GAL-VNE (Geng et al., 2023)	0.692 ± 0.028	0.567 ± 0.013	7.403 ± 0.345
CONAL	$\mathbf{0.781 \pm 0.027}$	$\mathbf{0.604 \pm 0.009}$	$\mathbf{9.458 \pm 0.161}$

worse compared to node ranking-based methods (e.g., GRC-GCN and NEA-VNE). The increased challenge of satisfying routing constraints in sparser topologies likely accounts for this performance discrepancy. These RL-based methods with less constraint awareness, result in a low solution feasibility guarantee and tend to exhibit lower performance. Meanwhile, CONAL still achieves the best performance, showing its effectiveness in these real-world network topologies.

G.5. Extension to Latency-aware VNE

In edge computing, latency is an additional quality of service (QoS) requirement, leading to a variant of VNE, known as latency-aware VNE. This variant incorporates latency constraints in addition to traditional VNE requirements. Specifically, a constraint is introduced for link mapping, where the total latency of the physical links in a path $p_p = f_L(l_v)$ routing virtual link l_v must not exceed the latency requirement of l_v. If any virtual link fails to meet its latency requirement, the VN request is rejected. Similar to previous studies (Jin et al., 2020; Adoga & Pezaros, 2023), we randomly assign coordinates to each physical node in the WX100 topology used in the main experiments, where each node represents a network edge. The latency for each physical link is then calculated based on the distance between paired physical nodes, and is normalized to a range of [0, 100] ms. For each VN request, the latency requirements of its virtual links are uniformly distributed within the range of [100, 500] ms. All other experimental settings remain consistent with those in the main experiments. To optimize these multi-type constraints, CONAL employs separate Lagrange multipliers for both resource and latency constraints, which are simultaneously managed by the neural lambda network Λ.

Table 4 presents the experimental results in latency-aware VNE. We observe that CONAL significantly outperforms all baseline methods, achieving the highest VN_RAC (0.781), LT_R2C (0.604), and LT_REV (9.458). Notably, the performance

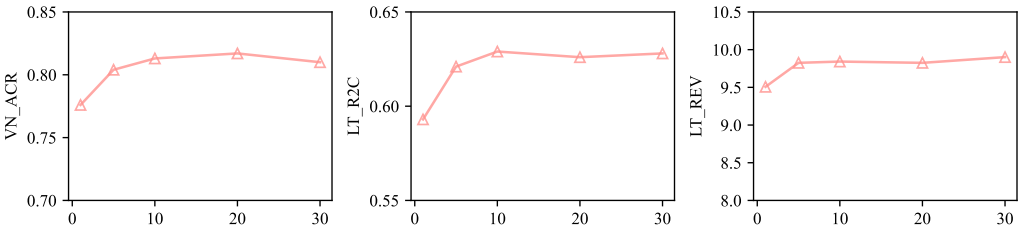

(a) VN Acceptance Rate (b) Long-term Revenue (c) Long-term R2C Ratio

Figure 10: The impact of update interval μ of surrogate policy proposed in the ARB method.

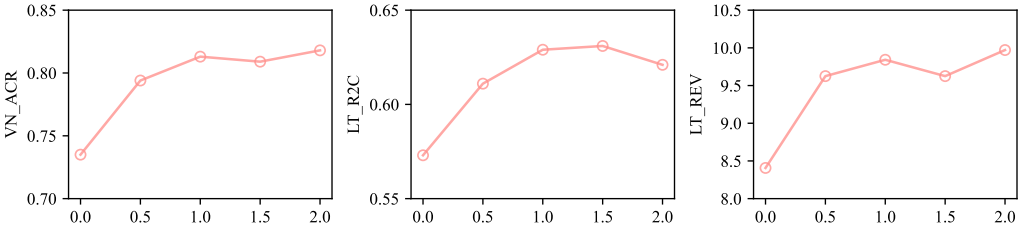

(a) VN Acceptance Rate (b) Long-term Revenue (c) Long-term R2C Ratio

Figure 11: The impact of augument ratio ϵ used in the path-bandwidth contrast module.

of GAL-VNE drops dramatically compared to the main experiment, even performing worse than the heuristic NEA-VNE. This is primarily because GAL-VNE relies on a one-shot solving paradigm and cannot effectively manage procedural delay constraints. In contrast, CONAL consistently maintains superior performance, thanks to its constraint-aware graph representation and adaptive optimization techniques, which balance both resource and latency constraints. These results highlight CONAL's robust handling of complex edge computing scenarios for latency-aware VNE, making it an extensible solution for variations in diverse networking paradigms.

G.6. Hyperparameter Impact Study

In this section, we explore the impact of two proposed key hyperparameters on the performance of CONAL, including the update interval μ of surrogate policy proposed in the ARB method and the augment ratio (ϵ) used in the path-bandwidth contrast module.

The impact of update interval of surrogate policy. This parameter μ controls the update interval of surrogate policy π' during training. We vary μ within the range [1, 5, 10, 20, 30] to explore its impact on key performance metrics, as shown in Figure 10. We observe that increasing μ initially leads to an improvement in all metrics. This suggests that extremely frequent updates of the surrogate policy make the budget values change rapidly, potentially leading to instability and divergence in the learning process. As μ increases beyond nearly 10, the improvements across these metrics tend to be stable and show minimal variation. This implies that while a moderate update interval enhances the model's performance, too-slow updates do not offer a significant further improvement on performance and may even increase computational overhead for training.

The impact of the augment ratio. This parameter determines the proportion of links to be added based on the number of nodes in the network. We change the augment ratio ϵ within the range [0, 0.5, 1.0, 1.5, 2.0] and the results are illustrated in Figure 11. As the augment ratio initially increases from 0 to 1.0, we observe improvements across performance metrics. However, when the augment ratio is increased beyond 1.0, these improvements become marginal or even negative. This indicates that excessive enhancement of the graph structure can increase learning difficulty. The increasing disparity between the enhanced and original graph topologies may also negatively impact performance. This study reveals that a reasonable augment ratio ϵ benefits the model by improving its sensitivity to bandwidth constraints. However, excessively high ϵ values provide only slight improvements or can even degrade performance. Generally, setting ϵ = 1.0 or a value close to it provides a balanced trade-off between performance enhancement and model robustness.

H. Used Benchmark and Assets

In this work, we list the used assets along with their version and license as follows:

- **Virne** is a widely-adopted VNE benchmarking library, offering many heuristic and machine learning-based methods for VNE. The source code can be accessed at https://github.com/GeminiLight/virne. It is licensed under Apache 2.0. In this work, we derived baseline implementations from Virne and developed our method using this library.
- **SNDlib** is a well-known library for telecommunication network design, which offers a collection of realistic network system topologies. This library is open-source and available at https://sndlib.put.poznan.pl, although the specific licensing terms are not clearly stated. In our real-world network validation (see Appendix G.4), we utilize network topologies such as GEANT and BRAIN, which are from SNDlib.